NOS1 mutations cause hypogonadotropic hypogonadism with sensory and cognitive deficits that can be reversed in infantile mice

Authors: Konstantina Chachlaki [1,2,3,4,5] *, Andrea Messina [3,4] *, Virginia Delli[1,2 Ψ], Valerie Leysen [1,2 Ψ], Csilla Maurnyi [6], Chieko Huber [7], Gaëtan Ternier[1, 2], Katalin Skrapits [6], Georgios Papadakis [3,4], Sonal Shruti [1,2¶], Maria Kapanidou [8], Xu Cheng [3,4§], James Acierno [3,4], Jesse Rademaker [3,4], Sowmyalakshmi Rasika [1,2], Richard Quinton [9], Marek Niedziela [10], Dagmar L'Allemand [11], Duarte Pignatelli [12], Mirjam Dirlewander [13], Mariarosaria Lang-Muritano [14], Patrick Kempf [15], Sophie Catteau-Jonard [1,2,16], Nicolas J. Niederländer [3,4], Philippe Ciofi [17], Manuel Tena-Sempere [18-20], John Garthwaite [21], Laurent Storme [2,22], Paul Avan [23], Erik Hrabovszky [6], Alan Carleton [7], Federico Santoni [3,4], Paolo Giacobini [1, 2], Nelly Pitteloud [3,4 ©*], Vincent Prevot [1, 2 ©*]

Affiliations:

[1] Univ. Lille, Inserm, CHU Lille, Laboratory of Development and Plasticity of the Neuroendocrine Brain, Lille Neuroscience and Cognition, UMR-S 1172, F-59000 Lille, France

[2] FHU 1000 days for Health, School of Medicine, F-59000 Lille, France

[3] Service of Endocrinology, Diabetology, and Metabolism, Lausanne University Hospital, 1011 Lausanne, Switzerland

[4] Faculty of Biology and Medicine, University of Lausanne, Lausanne 1005, Switzerland

[5] University Research Institute of Child Health and Precision Medicine, National and Kapodistrian University of Athens, "Aghia Sophia" Children's Hospital, 115 27 Athens, Greece

[6] Laboratory of Reproductive Neurobiology, Institute of Experimental Medicine, 43 Szigony St., Budapest 1083 Hungary

[7] Department of Basic Neurosciences, Faculty of Medicine, University of Geneva, 1 rue Michel-Servet, 1211 Geneva, Switzerland

[8] Department of Biological and Medical Sciences, Faculty of Health and Life Sciences, Oxford Brookes University, Oxford OX3 0BP, UK

[9] Translational & Clinical Research Institute and the Royal Victoria Infirmary, University of Newcastle-upon-Tyne NE1 3BZ, UK

[10] Department of Paediatric Endocrinology and Rheumatology, Poznan University of Medical Sciences, 61-701 Poznan, Poland.

[11] Department of Endocrinology, Children's Hospital of Eastern Switzerland, 9000 St. Gallen, Switzerland

[12] Department of Endocrinology, Hospital S João; Department of Biomedicine, Faculty of Medicine of the University of Porto; IPATIMUP Research Institute, 4200-319 Porto, Portugal

[13] Pediatric Endocrine and Diabetes Unit, Children's Hospital, University Hospitals and Faculty of Medicine, Geneva, CH1205, Switzerland

[14] Division of Pediatric Endocrinology and Diabetology and Children's Research Centre, University Children's Hospital, 8032 Zurich, Switzerland

[15] Department of Diabetes, Endocrinology, Clinical Nutrition & Metabolism, Inselspital, Bern University Hospital, University of Bern, 3010 Bern, Switzerland

[16] Department of Gynaecology and Obstretic, Jeanne de Flandres Hospital, Centre Hospitalier Universitaire de Lille, F-59000 Lille, France

[17] Inserm, U1215, Neurocentre Magendie, Université de Bordeaux, F-33077 Bordeaux, France

[18] Department of Cell Biology, Physiology and Immunology, University of Cordoba, 14004 Cordoba, Spain.

[19] Instituto Maimonides de Investigación Biomédica de Cordoba (IMIBIC/HURS), 14004 Cordoba, Spain.

[20] CIBER Fisiopatología de la Obesidad y Nutrición, Instituto de Salud Carlos III, 14004 Cordoba, Spain.

[21] The Wolfson Institute for Biomedical Research, University College London, London WC1E 6DH, UK

[22] Department of Neonatology, Hôpital Jeanne de Flandre, CHU of Lille, F-59000, France

[23] Université de Clerremont-Ferrand, F-63000 Clermont-Ferrand, France

*, [Ψ]   These authors contributed equally

¶Present address: Gene Therapy Process Sciences, UCB Pharma S.A., 1420 Braine l'Alleud, Belgium

§Present address: Renal Physiology Lab, Toronto General Hospital, University Health Network, Toronto, ON M5G 2C4, Canada

© *Corresponding authors*: Vincent Prevot (Vincent.prevot@inserm.fr; and Nelly Pitteloud (Nelly.Pitteloud@chuv.ch)

2

2

One-sentence summary:

4

The congenital GnRH deficiency caused by altered NOS1 activity can be rescued in mice

6   by nitric oxide therapy at minipuberty.

8

Editor's summary:

10

Abstract

12   The nitric oxide (NO) signaling pathway in hypothalamic neurons plays a key role in the regulation of the secretion of gonadotropin-releasing hormone (GnRH), which is crucial for

14   reproduction. We hypothesized that a disruption of neuronal NO synthase (NOS1) activity underlies some forms of hypogonadotropic hypogonadism. Whole exome sequencing

16   was performed on a cohort of 341 probands with congenital hypogonadotropic hypogonadism to identify ultra-rare variants in *NOS1*. The activity of the identified NOS1

18   mutant proteins was assessed by their ability to promote nitrite and cGMP production in vitro. In addition, physiological and pharmacological characterization was carried out in a

20   *Nos1*-deficient mouse model. We identified 5 heterozygous *NOS1* loss-of-function mutations in 6 probands with congenital hypogonadotropic hypogonadism (2%), who

22   displayed additional phenotypes including anosmia, hearing loss and intellectual disability. NOS1 was found to be transiently expressed by GnRH neurons in the nose of both

24   humans and mice, and *Nos1* deficiency in mice resulted in dose-dependent defects in sexual maturation as well as in olfaction, hearing and cognition. The pharmacological

26   inhibition of NO production in postnatal mice revealed a critical time window during which Nos1 activity shaped minipuberty and sexual maturation. Inhaled NO treatment at

28   minipuberty rescued both reproductive and behavioral phenotypes in *Nos1*-deficient mice. In summary, the lack of NOS1 activity led to GnRH deficiency associated with sensory

30   and intellectual comorbidities in humans and mice. NO treatment during minipuberty reversed deficits in sexual maturation, olfaction and cognition in Nos1 mutant mice,

32   suggesting a potential therapy for humans with NO deficiency.

Introduction

Pulsatile secretion of gonadotropin-releasing hormone (GnRH) is critical for the activation of the hypothalamic-pituitary-gonadal (HPG) axis, which controls pubertal onset and fertility. The HPG axis is transiently activated during late fetal development and again during early infancy, a phenomenon termed "minipuberty", remains dormant during childhood, and is then reactivated during puberty onset.

Congenital hypogonadotropic hypogonadism (CHH) is a rare genetic form of GnRH deficiency characterized by failure of puberty and infertility. CHH is associated with anosmia in about 50% of cases, in which case it is termed Kallmann syndrome (KS) (*1*). Other phenotypes such as sensorineural hearing loss (*2*), skeletal defects and cognitive or mental disorders (*3, 4*) also occur in CHH with variable frequencies. Although rarely studied, the transient HPG axis activation during minipuberty is also thought to be altered in CHH (*1*). The consequences of altered minipuberty are largely unknown beyond defects in testicular descent and penile growth (*5, 6*). However, preclinical studies in rodents show that it could not only impact the timing of puberty and reproductive fitness, given that multiple switches are being flipped during minipuberty to induce the mature pattern of GnRH release and correct fertility initiation, but could also affect cognitive abilities (*7-9*).

Mutations in more than 40 genes, acting either alone or in combination, have been identified in 50% of cases of CHH (*10*). Inactivating mutations in GnRH (*GNRH1*) (*11*) or GnRH receptor (*GNRHR*) (*12*) confirm the essential role of GnRH in reproduction. Furthermore, identification of mutations in other CHH genes (*1*) has been critical to unraveling the complex biological processes affecting GnRH neuronal fate specification, migration during embryonic development and GnRH secretion and action in adulthood (*1*). Of these, inactivating mutations in genes encoding kisspeptin (*KISS1*) (*13*) and its receptor (*KISS1R*) (*14, 15*) have pinpointed the kisspeptin system as a potent upstream activator of GnRH neurons (*1*). Hypothalamic kisspeptin neurons are estradiol-sensitive and convey feedback from gonadal steroids to GnRH neurons, an action that requires the priming of

the latter by nitric oxide (NO) release (*16*). Kisspeptin also directly acts on NO synthase

62   (Nos1) neurons, another estrogen-responsive population regulating GnRH neurons (*17,*

18).

64   NO acts by stimulating the production of cyclic guanosine monophosphate (cGMP) and is

involved in a wide range of biological processes in both humans and mice, including

66   neuronal development and plasticity (*19, 20*). The duration and intensity of NO signaling

are modulated by phosphodiesterases (PDEs), which hydrolyze cGMP (*21*). In the

68   hypothalamus, neuronal NO acts on GnRH neurons as an inhibitory signal that integrates

both metabolic and gonadal information (*21*). In addition, *Nos1*-deficient mice exhibit

70   infertility (*22*). We thus hypothesized that loss-of-function mutations in *NOS1* could lead

to GnRH deficiency and CHH by affecting key hypothalamic neuronal circuits controlling

72   fertility.

74   **Results**

NOS1 is produced by neurons in the fetal and adult human hypothalamus

76   We examined NOS1 abundance during prenatal development and in adult humans using

immunohistochemistry. In the nose of human fetuses, NOS1 was observed in some

78   migrating GnRH neurons but disappeared once they reached the forebrain region (Fig.

1A).

80   In adult patient brains, NOS1-producing neurons were widely distributed in the

hypothalamus (fig. S1A), intermingling and interacting morphologically with GnRH-

82   producing neurons at various sites, including the infundibulum (Fig. 1A, fig. S1B).

However, GnRH-producing neurons consistently did not co-express NOS1. Both NOS1-

84   producing and GnRH-producing neurons received input from kisspeptin-producing

neurons (Fig. 1, B to D). A subset (11.4±3.0%) of kisspeptin neurons also produced NOS1

86   (Fig. 1D), a phenomenon not seen in mice, in which Nos1 immunoreactivity was absent in

6

neurons expressing the neurokinin B receptor NK3R (fig. S1C), used as a surrogate to

88   identify kisspeptin-producing neurons in the arcuate nucleus of the hypothalamus (*23*).

90   **Six patients with CHH harbor heterozygous *NOS1* mutations**

NOS1 is a 29-exon gene encoding NOS1α, a 150 kDa protein consisting of 1434 amino

92   acids (GenBank: NM_000620.4) that functions as a homodimer (*24*). NOS1α is the most

commonly occurring isoform in the nervous system (*21*). Through whole exome

94   sequencing of a large cohort of unrelated patients with CHH (n = 341), we identified five

ultra-rare heterozygous *NOS1* missense variants in six probands (~2%) (Table 1; Table

96   S1; Fig. 2). None of the probands harbored pathogenic or likely pathogenic variants in

known CHH genes, according to the ACMG classification. Lastly, *NOS1* missense variants

98   were significantly enriched in our CHH cohort compared to the gnomAD control database

(two-sided Fisher's exact test, P = 2.64 × 10^{-2}).

100

The identified NOS1 mutants mapped to highly constrained sub-regions of NOS1 critical

102 for protein function (Fig. 2, A and B). Three variants (p.Thr1107Met, p.Glu1124Lys and

p.Ile1223Met) were located in the C-terminal reductase domain, critical for the catalytic

104 activity of the protein. More specifically, p.Ile1223Met was located in the nicotinamide

adenine dinucleotide (NAD)-binding pocket and the p.Thr1107Met and p.Glu1124Lys in

106 the flavin adenine dinucleotide (FAD)-binding pocket, both essential for electron transfer

to the oxygenase domain of the adjacent subunit of the dimer, leading to NO formation

108 (*24*). The p.Ala231Thr mutation lay within a regulatory region, the protein inhibiting NOS1

(PIN)-binding domain, whereas p. Arg260Gln was located in a low-complexity region

110 between the PIN-binding and oxygenase domains (Fig. 2A).

112 The p.Glu1124Lys *NOS1* mutation was identified in two unrelated probands—a female

patient with KS and a male patient with normosmic CHH (nCHH). The other four mutations

114 were found in 2 probands with KS and 2 probands with nCHH (Table 1).

CHH probands with NOS1 mutations frequently display comorbidities

The relevant clinical characteristics of the six probands are described here and summarized in Table 1. Four of six probands were male. All patients presented with absent puberty, suggesting severe GnRH deficiency. One male proband had a history of cryptorchidism and micropenis, consistent with altered minipuberty. DNA from family members was available in four cases. All probands inherited their mutations from unaffected or partially affected parents (Fig. 2B). In Family D, the female proband (II-1) harboring a p.Glu1124Lys *NOS1* mutation exhibited KS and inherited the *NOS1* mutation from her father (I-1), who suffered from constitutional delay of growth and puberty (CDGP), a transient form of GnRH deficiency (*25*). Hyposmia in the patient together with the presence of anosmia in her mother suggests oligogenic inheritance, although no other genetic defects in known CHH genes were identified in this pedigree (*1*). In addition, the male proband with KS in Family B exhibited anosmia, whereas the male proband with CHH in Family C exhibited hyposmia. Two probands with CHH (Family E, male, and Family F, female) displayed hearing loss, and one of them (Family F) also exhibited intellectual disability.

NOS1 mutants are loss-of-function

Before testing the enzymatic activity of the NOS1 mutants identified above *in vitro*, we first assessed their ectopic expression after transient transfection of HEK293 cells with tagged wild-type (WT) and mutant *NOS1* cDNA. Western blot analysis revealed that, in contrast to the WT construct, Thr1107Met and Glu1124Lys mutants were barely detected, suggesting disrupted protein synthesis or rapid degradation (Fig. 2C).

Consistent with altered expression, calcium-induced NO release using live-cell imaging was abrogated in cells transiently expressing Thr1107Met and Glu1124Lys mutants, and significantly attenuated for the 3 other reported mutants compared to cells expressing the WT plasmid ($P < 0.001$; Fig. 2, D to F; fig. S2, A and B), suggesting decreased NOS1

8

activity. NOS1 requires homodimerization to enzymatically convert L-arginine and oxygen into L-citrulline and NO (*26*), and NOS1 mutants can impair the formation of active NOS1 dimers, resulting in reduced NO production *in vitro* (*27*). The decreased enzymatic activity of mutants was further confirmed using a fluorometric nitrate kit (fig. S2C). To test the possibility that NOS1 mutants impair the activity of NOS1 dimers by heterodimerizing with the NOS1 produced by the WT allele, we generated bicistronic constructs producing equimolar amounts of WT and mutated *NOS1* transcripts (fig. S2D). NOS1 activity *in vitro* was diminished to the same extent by the biscistronic construct as when cells were transfected with the mutants alone (fig. S2C), and mutant isoforms were seen to co-immunoprecipitate with WT isoforms (Fig. 2G), demonstrating that the *NOS1* mutants identified in our patients are dominant negative.

NOS1 modulates GnRH neuron number and migration

NO is implicated in the regulation of neuronal migration in the brain during mouse embryogenesis (*19*). We thus explored the involvement of NOS1 in GnRH neuronal migration. In mouse embryos at embryonic day (E) 14.5, GnRH-producing neurons co-expressed Nos1 in the nose but not the forebrain (Fig. 3A). Next, we induced a transient and site-specific inhibition of NO production by infusing the NOS inhibitor N(G)-Nitro-L-arginine methyl ester (L-NAME) locally into the nasal region of WT mouse embryos on E12.5, when GnRH-producing cells start to enter the rostral forebrain (Fig. 3B). Inhibiting NO production at E12.5 resulted in a substantial alteration in migration (Fig. 3, C and D); at E14.5, the majority of GnRH-producing neurons, which formed part of Nos1-immunolabeled aggregates, were arrested in the nose before entering the brain, skewing the distribution of the neurons (Fig. 3, C and D). However, the total number of GnRH neurons in whole heads, that is, in both the nose and the brain, at E14.5 appeared higher in L-NAME-treated embryos than in littermates treated with saline in the contralateral horn of the dam's uterus (Fig. 3E). To better understand the role of Nos1 in GnRH-producing neuron migration, we evaluated the distribution and total number of GnRH-producing

neurons in the whole head, that is, in the nose (yellow, Movie S1) and the brain (red, Movie

172   S1) (Fig. 3F) of neonatal (P0) mice lacking exon 2 of *Nos1* (*Nos1$^{-/-}$* mice) (*28*), using three-

dimensional (3D) imaging and analysis of solvent-cleared tissue (iDISCO), which we have

174   previously shown can accurately count GnRH immunolabeled neurons in the whole brain

(*29*). Contrary to the effect of NOS inhibition by L-NAME in E14.5 embryos (Fig. 3, D and

176   E), the distribution of GnRH somata at birth did not differ between *Nos1$^{-/-}$* mice and WT

littermates (Fig. 3G, Movie S2). However, similar to L-NAME-injected E14.5 embryos (Fig.

178   3E), *Nos1$^{-/-}$* mice showed higher total numbers of GnRH-producing neurons at P0 (Fig.

3H), suggesting that Nos1 activity may, at least in part, control the size of this neuronal

180   population. Lastly, transient axonal glycoprotein 1 (TAG-1) immunoreactivity showed that

olfactory bulb morphogenesis and olfactory and vomeronasal fiber projections to the

182   olfactory bulb were not altered in *Nos1$^{-/-}$* mice (Fig. 3I), suggesting preserved connectivity

between the nasal epithelium and the brain in this mouse model of Nos1 deficiency.

184

Nos1-deficient mice show altered sensory and cognitive performance

186   The presence of associated phenotypes such as anosmia, hearing loss and mental

retardation in CHH patients harboring heterozygous *NOS1* mutations (Table 1) led us to

188   evaluate these traits in *Nos1$^{-/-}$* mice, in which Nos1 activity is markedly impaired although

some residual activity persists (*28*).

190   During the social odor discrimination test, both *Nos1$^{-/-}$* and *Nos1$^{+/-}$* mice failed to be

attracted by volatile urine odors of the opposite sex (Fig. 4A). During the habituation-

192   dishabituation test, both *Nos1$^{-/-}$* and *Nos1$^{+/-}$* mice could discriminate new non-social odors

(Fig. 4B). However, *Nos1$^{-/-}$* mice were hyper-reactive to these stimuli (Fig. 4B), similar to

194   what has been observed in premature infants during a visual habituation-dishabituation

task (*30, 31*). The alteration of the sense of smell in *Nos1*-deficient mice thus consists of

196   a sex-independent impairment in the encoding or processing of non-social olfactory

information without gross defects in odor detection (that is, no general anosmia).

10

We studied hearing in *Nos1*-deficient mice by measuring distortion-product otoacoustic emissions. Male, but not female, *Nos1*^{-/-} mice exhibited defects in the auditory pathway at the level of the cochlear nucleus as shown by an increased latency in the auditory brainstem-evoked response (ABR) wave II (Fig. 4C), and mean threshold elevations of 18.9 dB at 40 kHz (Fig. 4D).

Both *Nos1*^{-/-} and *Nos1*^{+/-} mice demonstrated defective cognitive performance compared to WT littermates in the novel object recognition test (Fig. 4E). We next tested executive functions and cognitive flexibility in *Nos1*^{-/-} mice and their WT littermates using the attentional set-shifting task (*32-34*) (ASST) (Fig. 4F), which relies on a sequence of blocks (each composed of individual trials) testing different cognitive states; each block must be completed before moving on to the next. The simple discrimination (SD) and compound discrimination (CD, in which one type of sensory information serves as a distractor from another) blocks test basic perceptual and associative abilities. The compound discrimination-reversal (CDR) block measures the ability to adjust behavior for previously learned cue-reward contingencies. The intradimensional set-shifting (IDS) block assesses attentional set formation and maintenance, whereas the extradimensional set-shifting (EDS) block assesses the cognitive flexibility required to disengage from previously relevant information and shift attention towards a newly relevant stimulus.

All *Nos1*^{+/+} and *Nos1*^{-/-} mice were able to complete all blocks of the ASST, with response latency being similar between genotypes (Fig. 4G). Although the required number of trials to complete each block did not change between groups (Fig. 4I), the pattern across blocks differed between genotypes. *Nos1*^{+/+} mice needed fewer trials to complete the IDS block than the CD block, and required more trials for the EDS block than the IDS block (Fig. 4I), as previously reported for such tests (*32-34*), reflecting the formation of an attentional set and cognitive flexibility. *Nos1*^{+/+} mice also needed more trials to complete the CDR block than the CD block and displayed lower response accuracy (Fig. 4, H and I), in keeping with the increased number of trials required to suppress a previously learned cue-reward contingency due to perseverative errors (*32-34*). *Nos1*^{-/-} mice did not exhibit such a pattern

226 or any sign of attentional set formation (Table S2), but seemed to solve each block

independently of past experience. Moreover, $Nos1^{-/-}$ mice did not show any difference in

228 the number of trials needed to complete the CDR block versus the CD block, and

committed fewer perseverative errors than $Nos1^{+/+}$ mice (Fig. 4, I and J). Overall, their

230 learning curves did not differ between the two blocks, again suggesting that $Nos1^{-/-}$

mutants treated them independently (Fig. 4K). In summary, $Nos1^{-/-}$ mice displayed normal

232 basic perceptual and associative abilities but impaired cognitive abilities such as reversal

learning and attentional set formation.

234

Infantile Nos1 activity shapes minipuberty

236 Although it is known that $Nos1^{-/-}$ mice exhibit central reproductive defects and infertility

(*22*), the underlying mechanisms are largely unknown. In a recent study, we demonstrated

238 that Nos1 activity increases in the preoptic region, including the organum vasculosum of

the lamina terminalis (OVLT), during the infantile period (*7*), known to be crucial for the

240 establishment of the GnRH neural network (*8, 21, 35*). Most hypothalamic Nos1-

expressing neurons in mice lie in the OVLT region (*17*), where GnRH-expressing neuronal

242 cell bodies and dendrites also reside (*17*). We therefore measured immunoreactivity for

Ser1412 phosphorylation-activated Nos1 (P-Nos1) (*36*) in the OVLT at neonatal (P7),

244 infantile (P10 and P12) and post-weaning (P23) stages (Fig. 5A and fig. S3, A and B). The

proportion of Nos1 neurons expressing P-Nos1 increased at P12 (Fig. 5A), when high

246 circulating follicle stimulating hormone (FSH) concentrations signal the occurrence of

minipuberty in infantile mice (*7*), and persisted thereafter (Fig. 5A). P-NOS1

248 immunoreactivity was also found in the hypothalamus of men and in women both of

childbearing age and after menopause (fig. S3C). To determine whether this infantile

250 increase in P-Nos1 could be linked to the FSH-induced estrogen output from the ovaries

(*37*), we analyzed P-Nos1 expression in P23 WT mice after ovariectomy at P12, and found

252 a marked loss of P-Nos1 immunoreactivity in the OVLT (Fig. 5, A and B, fig. S3A) as well

as the hippocampus (36.2±5.9% *vs.* 10.4±2.4% P-Nos1-immunoreactive Nos1-expressing neurons, *n*=3 and 4 per group, respectively, *P* =0.006; fig. S3B).

Because NO is known to restrain GnRH neuronal activity (*21, 38*), we next performed electrophysiological analyses in *Nos1*-deficient females at minipuberty. As expected, spontaneous firing in infantile GnRH-producing neurons was markedly increased during the third week of life in *Gnrh*::*Gfp*; *Nos1*$^{-/-}$ mice, compared to their *Gnrh*::*Gfp*; *Nos1*$^{+/+}$ littermates (Fig. 5C and fig. S4). This increase was associated with a 4-fold increase in GnRH transcripts in *Nos1*-deficient mice compared to WT littermates at P12 rather than by P23, as shown using real-time PCR analyses of GnRH-producing neurons after fluorescence-activated cell sorting (Fig. 5D). Recent data have implicated infantile NO in *Gnrh* promoter activity during minipuberty via the transcription factor CCAAT/enhancer binding protein (C/EBP) β (*7*). Transcripts for the C/EBPβ gene, *Cebpb*, were downregulated in GnRH-producing neurons isolated from Nos1-deficient mice (fig. S5A), suggesting that, in addition to regulating the C/EBPβ-mediated repression of the *Gnrh* promoter (*7, 39*), neuronal NO could also be involved in controlling the expression of this *Gnrh* promoter repressor itself. Both the increase in spontaneous firing by infantile GnRH-producing neurons and GnRH expression (Fig. 5, C and D) were consistent with increased GnRH release, as shown by elevated luteinizing hormone (LH) and FSH levels in *Nos1*-deficient female mice at P12 (Fig. 5, E and F). Although concentrations of FSH after weaning reached their nadir at P23 in WT mice, they remained abnormally high in *Nos1*-deficient mice and only reached control concentrations by P30 (Fig. 5E). In contrast, LH concentrations at minipuberty were elevated in both *Nos1*$^{-/-}$ and *Nos1*$^{+/-}$ mice and reached WT levels at P23 (Fig. 5F). While *Gnrh1* transcripts in the pituitary were unchanged (fig. S5B), these aberrant gonadotropin levels in Nos1-deficient mice were associated with blunted estradiol concentrations during the infantile period (Fig. 5G) and increased inhibin B concentrations at P23 (Fig. 5H), but unaltered circulating anti-Mullerian hormone (AMH) (Fig. 5I). Combined, these results suggested that increased Nos1 activity during

280 minipuberty is required for the hypothalamus-driven onset of gonadal steroid negative feedback and the repression of the HPG axis at the end of minipuberty.

282

Puberty is altered in *Nos1*-deficient mice

284 The first external signs of sexual maturation, vaginal opening and first ovulation in females and balanopreputial separation in males, were altered in $Nos1^{-/-}$ mice (Fig. 6, A to C).

286 Vaginal opening was also delayed in $Nos1^{-/+}$ females (Fig. 6A). These defects were associated with abnormal estrous cyclicity and sporadic ovulatory events in young adult

288 $Nos1^{-/-}$ mice (Fig. 6D).

Pharmacologically-induced infantile NO deficiency alters sexual maturation

290 To further explore the physiological role of infantile NO in the maturation of the

292 reproductive axis, we specifically inhibited NO production in WT mice between P10 and P21 by the daily intraperitoneal injection of L-NAME (50 mg/kg). This pharmacologically-

294 induced infantile NO deficiency (Fig. 6, E to H) recapitulated the reproductive phenotype of genetic *Nos1*-deficient mice (Fig. 6, A to D), with delayed vaginal opening (Fig. 6E) and

296 pubertal onset (Fig. 6F). Furthermore, infantile NO deficiency led to a deficit in adult reproductive capacity, as indicated by an increased percentage of days spent in diestrus

298 and fewer successful ovulatory events (Fig. 6G). The typical preovulatory LH surge in adulthood (P75-90) was also blunted in most infantile-NO-deficient mice (Fig. 6H) when

300 compared to vehicle-treated animals. When NO production was abolished at P7-P12, an early infantile period when FSH levels are rising (*35*), there was no effect on sexual

302 maturation despite an effect on postnatal growth (fig. S6, A and B), clearly defining the P10-P21 period as a critical window for the action of infantile NO.

304

Altered sexual maturation, olfactory, and cognitive impairments in *Nos1*-deficient mice are

306 **rescued by treatment with NO or sildenafil**

14

We next investigated whether inhaled NO (iNO) during this critical period could improve

308   the reproductive phenotype of *Nos1*-deficient mice. iNO during the P10-P23 period

rescued vaginal opening (Fig. 6A) and age at balanopreputial separation (Fig. 6B) in both

310   *Nos1*^{-/-} and *Nos1*^{+/-} mice, and it rescued pubertal onset in females (Fig. 6C), as well as

estrous cyclicity in adult *Nos1*^{-/-} females (Fig. 6D). Because the *Nos1*^{-/-} mouse model used

312   in this study exhibits some residual Nos1 activity (*28*), we next determined whether

treatment with the selective inhibitor of cGMP-specific PDE5, sildenafil, commonly used in

314   human neonates as an alternative to iNO (*40*), could also rescue the phenotype of these

mice. Daily sildenafil injections between P10 and P23 partially normalized sexual

316   maturation in *Nos1*^{-/-} mice (Fig. 6, A, C and D). Administration of iNO or sildenafil during

infancy in *Nos1*-deficient mice also restored olfactory (Figure 4A, B) and cognitive

318   impairments in adulthood (Figure 4E), demonstrating that these neurodevelopmental

alterations are at least partially related to Nos1 deficiency or its consequences.

320

Discussion

322   In this study, we identified several ultra-rare heterozygous mutations in highly constrained

subregions of *NOS1* in our CHH patient cohort (*41*). As with other CHH-associated genes

324   (*1, 42*), these were inherited from partially affected or unaffected parents in an autosomal

dominant fashion, suggesting segregation with variable expressivity and reduced

326   penetrance.

328   In mice, a total loss of Nos1 catalytic activity (i.e., deletion of the oxygenase domain)

results in centrally-mediated hypogonadism and infertility (*22*). Here, in *Nos1* knockout

330   mice lacking exon 2 [with some residual Nos1 activity (*28, 43*)], Nos1 deficiency dose-

dependently impaired puberty onset and fertility, as expected from the fact that Nos1

332   homodimerization is necessary for NO production (*26, 27*). This is consistent with the

markedly impaired *in vitro* activity of the heterozygous NOS1 mutants and the extreme

334   intolerance to *NOS1* loss-of-function mutations seen in CHH patients.

336   Although the hallmark of CHH is impaired puberty, minipuberty is also thought to be absent

in most patients (*44*). Occurring during the first postnatal months in humans (*45, 46*) and

338   the second week of life in rodents (*35*), minipuberty is characterized by a transient surge

in GnRH production leading to gonadal activation. In our genetically or pharmacologically

340   Nos1-deprived mice, minipuberty was exaggerated, with increased GnRH expression and

neuronal activity and abnormally elevated and sustained FSH levels. These early changes

342   delayed puberty and altered adult fertility, defining an infantile critical window during which

NO shapes the maturation of central neuroendocrine circuits driving pulsatile GnRH

344   release. Whether the dynamics of GnRH release during minipuberty also shapes puberty

onset and adult fertility in CHH or CDGP patients must be confirmed.

346

NOS1 is the first gene encoding a neurotransmitter-synthesizing enzyme to be implicated

348   in CHH. The increase in Nos1-dependent NO production in the hypothalamus and

hippocampus of infantile female mice appears to depend on hormones secreted by the

350   maturing gonads, likely estrogens (*47-49*), which promotes the establishment of neuronal

circuits in several other brain areas (*50-52*). Furthermore, sildenafil, used to treat erectile

352   dysfunction in men, increases serum testosterone (*53*), and in 10-20% of CHH patients,

hormone therapy to normalize their sex steroid milieu reverses their condition (*54*). Non-

354   reproductive deficits displayed by our probands, such as sensory deficits or intellectual

disability, are reproduced in *Nos1*-deficient mice, reflecting the NO-dependent impairment

356   of other neuronal circuits (*55-57*). NO may thus control the establishment and homeostasis

of both reproductive and non-reproductive neuronal networks, and the rise in FSH-induced

358   estrogen production during minipuberty (*58*) may trigger the synchronous maturation of

these varied Nos1-dependent networks.

360

Although anosmia in CHH was thought to result from the defective axonal targeting of

362   olfactory neurons, which contribute to the migratory scaffold for GnRH neurons (*1, 59, 60*),

olfactory projections were unaltered in *Nos1*$^{-/-}$ mice. Instead, suppressing Nos1 activity

364   during embryonic development perturbed GnRH neuronal migration from nose to brain,

consistent with a temporally restricted action of NO, but also led to more GnRH-expressing

366   neurons in the heads of newborn mice, suggesting that the migratory defect is either

transient or compensated for by increased GnRH neuron production. One explanation for

368   this increase is the modulation of GnRH expression by the C/EBPβ-NO-dependent

transcription-factor-gene micronetwork that represses the *Gnrh* promoter (*7*).

370   Alternatively, NO may also control GnRH neuronal survival through distinct signaling

pathways, including the semaphorin class 3 receptor, neuropilin-1 (*61*), recently shown to

372   promote GnRH-expressing neuronal death during embryogenesis (*62*). Additionally, the

fact that not all GnRH-expressing neurons express Nos1 suggests the existence of

374   multiple subpopulations of these neurons with different characteristics and distinct

responses to the absence of Nos1.

376

NO is also known to modulate neural activity and synaptic transmission in the olfactory

378   system (*63, 64*). NO-mediated cGMP production and enhanced glutamate release appear

involved in the brain plasticity underlying odor perception and olfactory memory formation

380   in various species (*65-68*). NO could also change olfactory neurogenesis and neuronal

migration during development (*69*), and fine-tune network activity and maturation during

382   embryonic and early postnatal development (*70, 71*). The olfactory processing deficits

seen in *Nos1*$^{-/-}$ mice and some KS patients could stem from aberrant synaptic plasticity or

384   neuronal circuit synchronization in the olfactory bulb by NO/cGMP signaling through

GABAergic interneurons (*66, 72, 73*). Several genes of the NO/cGMP pathway are located

386   in human deafness loci (*GUCY* encoding guanylate cyclase, *NOS1*, *NOS2*, and *NOS3*)

17

(*74, 75*), and auditory deficits, such as those of patients E and F, have been associated

388   with alterations in this pathway (*76, 77*).

390   Intellectual disability and cognitive deficits in CHH probands and *Nos1$^{-/-}$* mice, respectively, also may reflect a broader link between NO signaling and neurodevelopment. Our *Nos1$^{-/-}$*

392   mice displayed WT-like basic perceptual and associative abilities but impaired cognitive abilities due to deficient reversal learning and attentional set formation. The Fragile X

394   protein, FMRP (fragile X mental retardation 1 protein), whose loss of function is the leading monogenic cause of intellectual disability and autism, binds the *NOS1* transcript and

396   increases its translation in the developing neocortex (*72*). A hypomorphic *NOS1* allele is also associated with attention deficit hyperactivity disorder, impulsivity and aggression in

398   humans (*78*). Preterm infants, who have an increased risk of developing impaired reproductive capacity (*79*), intellectual disability and hearing loss (*80, 81*), also display

400   abnormally high serum FSH levels during minipuberty (*45, 46*), recapitulating some phenotypic aspects of *Nos1*-deficient CHH patients and mice.

402

Exogenous NO or sildenafil administration during minipuberty attenuated both

404   reproductive and non-reproductive phenotypes in our mice, confirming the crucial role played by NO. Given the safe use of both treatments to promote lung maturation and

406   vascularization in premature infants, this line of treatment between 1 and 6 months of age may be useful to improve brain development and future quality of life in infants born to

408   CHH patients with *NOS1* mutations.

410   Our study does have some limitations. Whether CHH patients with *NOS1* mutations undergo altered minipuberty is still being investigated by the European miniNO consortium

412   (https://www.minino-project.com). This project is also investigating whether iNO treatment at minipuberty could benefit infants at risk of developing sensory and cognitive alterations.

414   Additionally, although our study identified a critical period for the action of Nos1 on the

18

establishment of the HPG axis, NO is also involved in the function of reproductive and
416 non-reproductive neural circuits in adulthood (*21, 24*), and the effects of iNO or PDE5-inhibitors in adult mice and patients must be explored.

418

In summary, NO has long been known to play a role in the maturation and homeostasis of
420 the cardiovascular, immune and central nervous systems. Our study expands its spectrum of actions in the brain to include both cognitive development and the regulation of sexual
422 maturation and reproduction, and pinpoints minipuberty as a critical period for these actions.

Materials and Methods
424

Study design

426 This study was designed to investigate the role of NOS1 in reproductive neuroendocrine development and adult sensory and cognitive functions and was conducted in both
428 humans and mice. Permission to use 9 gestational-week-old human fetuses was obtained from the French Agence de Biomédecine (PFS16-002). Male and female adult human
430 hypothalamic tissues were obtained at autopsies from the Forensic Medicine Department of the University of Debrecen, Hungary, with the permission of the Regional Committee of
432 Science and Research Ethics (DEOEC RKEB/IKEB: 3183-2010). The study in patients was approved by the ethics committee of the University of Lausanne (CER-VD 345/11;
434 PB_2018-00247) and registered onto Clinicaltrials.gov with the number NCT01601171. All participants provided written informed consent prior to study participation.

436 All animal procedures were carried out in accordance with the guidelines for animal use specified by the European Union Council Directive of September 22, 2010 (2010/63/EU)
438 and were approved by the Institutional Ethics Committees for the Care and Use of Experimental Animals of the Universities of Lille, Bordeaux and Geneva, and the French
440 Department of Research (APAFIS#2617-2015110517317420v5 and #27300-

2020092210299373v3) and Geneva state ethics committees. Both sexes were used in this study. Investigators were blind to the experimental group, to which age- and sex-matched littermates were assigned according to their genotype. No study size calculation was performed. No data were excluded from the study.

Patients

The CHH cohort included 341 probands (184 KS and 173 normosmic CHH [nCHH]). The diagnosis of CHH was made on the basis of: i) absent or incomplete puberty by 17 years of age; ii) low/normal gonadotropin levels in a setting of low serum testosterone/estradiol levels; and iii) otherwise normal anterior pituitary function and normal imaging of the hypothalamic-pituitary region (*1*). Olfaction was assessed by self-reporting and/or formal testing (*82*). When available, family members were included for genetic studies. This study was approved by the ethics committee of the University of Lausanne. All participants provided written informed consent prior to study participation.

Genetic analyses

Genomic DNA was extracted from peripheral blood samples using the Puregene Blood Kit (Qiagen), following the manufacturer's protocol. Exome capture was performed using the SureSelect All Exon capture v2 or v5 (Agilent Technologies) and sequenced on the HiSeq2500 (Illumina) at BGI (BGI, Shenzen). Raw sequences (FASTQ files) were analyzed using an in-house pipeline that utilized the Burrows-Wheeler Alignment algorithm (BWA) (*83*) for mapping the reads to the human reference sequence (GRCh37), and the Genome Analysis Toolkit (GATK) (*84*) for the detection of single nucleotide variants (SNVs) and insertion/deletions (Indels). The resulting variants were annotated using Annovar version 20191024(*85*) and dbNSFP version 4.0(*86*) for minor allele frequency (MAF) and pathogenicity scores.

20

Based on the prevalence of CHH (*1*), we established the MAF threshold as 0.01% and excluded all variants with a higher MAF in gnomAD. Candidate *NOS1* variants were then prioritized using the following criteria: (1) *in silico* prediction of deleteriousness [CADD (*87*) > 15], and (2) variant position in sub-regions highly intolerant to variation (LIMBR) (*41*) score percentile < 5). All variants were confirmed by Sanger sequencing of both strands with duplicate PCR reactions. A gene burden analysis for the identified *NOS1* variants was performed using a two-tailed Fisher's exact test in CHH probands versus. controls (gnomAD exome controls). Furthermore, mutations in known CHH genes *(1)* according to ACMG criteria were noted for each proband and family members harboring rare variants in *NOS1*.

Studies of NOS1 expression

NOS1 expression was studied by immunohistochemistry in fetal heads and adult human hypothalamic tissues as described in the Supplementary Materials and Methods.

Studies of NOS1 abundance and signaling

A human embryonic kidney cell line (HEK 293T) was transiently co-transfected with each NOS1 mutant and the FlincG3 NO-detector plasmid (pTriEx4-H6-FGAm)(*88*) and subjected to live imaging to assess the concentration of NO released upon the application of the calcium ionophore A23187, as described in the Supplementary Materials and Methods. NOS1 mutants abundance, heterodimerization with WT NOS1 isoforms and activity were also assessed using alternative methods (see Supplementary Materials and Methods).

Assays in mice

Neuroanatomical analyses, electrophysiological recordings and gene expression analysis in GnRH-producing neurons, and examination of reproductive physiology and

behavioral testing were carried out in male and female *Nos1*-deficient (*Nos1*^{-/-},

494 B6.129S4-Nos1tm1Plh/J) mice (*28*) and their *Nos1*^{+/-} and *Nos1*^{+/+} littermates,

subjected or not to iNO (20ppm) or sildenafil (15mg/kg, intraperitoneally) treatment

496 during the infantile period (see the Supplementary Materials and Methods).

Statistical analyses

All analyses were performed using Prism 7 (GraphPad Software) and assessed for

500 normality (Shapiro–Wilk test) and variance, when appropriate. Sample sizes were chosen

according to standard practice in the field. The investigators were blind to group allocation

502 during the experiments. For each experiment, replicates are described in the figure

legends. For animal studies, data were compared using an unpaired two-tailed Student's

504 *t*-test or a one-way analysis of variance (ANOVA) for multiple comparisons against the

control condition followed by Dunnett multiple comparison *post-hoc* test. Data not following

506 normal distribution were analyzed using either a Mann-Whitney *U* test (comparison

between two experimental groups) or Wilcoxon/Kruskal-Wallis test (comparison between

508 three or more experimental groups) followed by a Dunn's *post hoc* analysis. The number

of biologically independent experiments, sample size, P values, age and sex of the

510 animals are all indicated in the main text or figure legends as well as in data file S1. All

experimental data are indicated as mean ± SEM. Significance was set at $P<0.05$. Symbols

512 in figures correspond to the following significance levels: *$P<0.05$, **$P<0.001$, ***$P <$

0.0001. Exact P values and further statistical analyses are provided in Table S2 and raw

514 data in Data file S1.

List of Supplementary Materials

516 Materials and Methods
Figures S1 to S7
518 Tables S1 to S3

22

MDAR reproducibility checklist

520   Movies S1 and S2

Data file S1

522   References *(88-108)*

524

References

526   1.   U. Boehm, P. M. Bouloux, M. T. Dattani, N. de Roux, C. Dode, L. Dunkel, A. A. Dwyer, P. Giacobini, J. P. Hardelin, A. Juul, M. Maghnie, N. Pitteloud, V.
528   Prevot, T. Raivio, M. Tena-Sempere, R. Quinton, J. Young, Expert consensus document: European Consensus Statement on congenital hypogonadotropic
530   hypogonadism--pathogenesis, diagnosis and treatment. *Nat Rev Endocrinol* **11**, 547-564 (2015); published online EpubSep (10.1038/nrendo.2015.112).

532   2.   V. Pingault, V. Bodereau, V. Baral, S. Marcos, Y. Watanabe, A. Chaoui, C. Fouveaut, C. Leroy, O. Verier-Mine, C. Francannet, D. Dupin-Deguine, F.
534   Archambeaud, F. J. Kurtz, J. Young, J. Bertherat, S. Marlin, M. Goossens, J. P. Hardelin, C. Dode, N. Bondurand, Loss-of-function mutations in SOX10 cause
536   Kallmann syndrome with deafness. *Am J Hum Genet* **92**, 707-724 (2013); published online EpubMay 2 (10.1016/j.ajhg.2013.03.024

538   S0002-9297(13)00162-6 [pii]).

        3.   U. Aydogan, A. Aydogdu, H. Akbulut, A. Sonmez, S. Yuksel, Y. Basaran, O.
540   Uzun, E. Bolu, K. Saglam, Increased frequency of anxiety, depression, quality of life and sexual life in young hypogonadotropic hypogonadal males and
542   impacts of testosterone replacement therapy on these conditions. *Endocr J* **59**, 1099-1105 (2012).

544   4.   L. Lasaite, J. Ceponis, R. T. Preiksa, B. Zilaitiene, Impaired emotional state, quality of life and cognitive functions in young hypogonadal men. *Andrologia*
546   **46**, 1107-1112 (2014); published online EpubDec (10.1111/and.12199).

        5.   T. Kuiri-Hanninen, U. Sankilampi, L. Dunkel, Activation of the hypothalamic-
548   pituitary-gonadal axis in infancy: minipuberty. *Horm Res Paediatr* **82**, 73-80 (2014)10.1159/000362414).

550   6.   L. Lanciotti, M. Cofini, A. Leonardi, L. Penta, S. Esposito, Up-To-Date Review About Minipuberty and Overview on Hypothalamic-Pituitary-Gonadal Axis
552   Activation in Fetal and Neonatal Life. *Front Endocrinol (Lausanne)* **9**, 410 (2018)10.3389/fendo.2018.00410).

554   7.   A. Messina, F. Langlet, K. Chachlaki, J. Roa, S. Rasika, N. Jouy, S. Gallet, F. Gaytan, J. Parkash, M. Tena-Sempere, P. Giacobini, V. Prevot, A microRNA
556   switch regulates the rise in hypothalamic GnRH production before puberty. *Nat Neurosci* **19**, 835-844 (2016); published online EpubJun (10.1038/nn.4298).

558   8.   G. Pellegrino, M. Martin, C. Allet, T. Lhomme, S. Geller, D. Franssen, V. Mansuy, M. Manfredi-Lozano, A. Coutteau-Robles, V. Delli, S. Rasika, D.
560   Mazur, A. Loyens, M. Tena-Sempere, J. Siepmann, F. P. Pralong, P. Ciofi, G. Corfas, A. S. Parent, S. R. Ojeda, A. Sharif, V. Prevot, GnRH neurons recruit
562   astrocytes in infancy to facilitate network integration and sexual maturation. *Nat Neurosci* **24**, 1660–1672 (2021); published online EpubNov 18
564   (10.1038/s41593-021-00960-z).

9.   M. Manfredi-Lozano, V. Leysen, M. Adamo, I. Paiva, R. Rovera, J. M. Pignat, F. E. Timzoura, M. Candlish, S. Eddarkaoui, S. A. Malone, M. S. B. Silva, S. Trova, M. Imbernon, L. Decoster, L. Cotellessa, M. Tena-Sempere, M. Claret, A. Paoloni-Giacobino, D. Plassard, E. Paccou, N. Vionnet, J. Acierno, A. M. Maceski, A. Lutti, F. Pfrieger, S. Rasika, F. Santoni, U. Boehm, P. Ciofi, L. Buee, N. Haddjeri, A. L. Boutillier, J. Kuhle, A. Messina, B. Draganski, P. Giacobini, N. Pitteloud, V. Prevot, GnRH replacement rescues cognition in Down syndrome. *Science* **377**, eabq4515 (2022); published online EpubSep 2 (10.1126/science.abq4515).

10.   D. Cassatella, S. R. Howard, J. S. Acierno, C. Xu, G. E. Papadakis, F. A. Santoni, A. A. Dwyer, S. Santini, G. P. Sykiotis, C. Chambion, J. Meylan, L. Marino, L. Favre, J. Li, X. Liu, J. Zhang, P. M. Bouloux, C. Geyter, A. Paepe, W. S. Dhillo, J. M. Ferrara, M. Hauschild, M. Lang-Muritano, J. R. Lemke, C. Fluck, A. Nemeth, F. Phan-Hug, D. Pignatelli, V. Popovic, S. Pekic, R. Quinton, G. Szinnai, D. l'Allemand, D. Konrad, S. Sharif, O. T. Iyidir, B. J. Stevenson, H. Yang, L. Dunkel, N. Pitteloud, Congenital hypogonadotropic hypogonadism and constitutional delay of growth and puberty have distinct genetic architectures. *Eur J Endocrinol* **178**, 377-388 (2018); published online EpubApr (10.1530/EJE-17-0568).

11.   J. Bouligand, C. Ghervan, J. A. Tello, S. Brailly-Tabard, S. Salenave, P. Chanson, M. Lombes, R. P. Millar, A. Guiochon-Mantel, J. Young, Isolated familial hypogonadotropic hypogonadism and a GNRH1 mutation. *N Engl J Med* **360**, 2742-2748 (2009); published online EpubJun 25 (10.1056/NEJMoa0900136).

12.   N. de Roux, J. Young, M. Misrahi, R. Genet, P. Chanson, G. Schaison, E. Milgrom, A family with hypogonadotropic hypogonadism and mutations in the gonadotropin-releasing hormone receptor. *N Engl J Med* **337**, 1597-1602 (1997); published online EpubNov 27 (10.1056/NEJM199711273372205).

13.   A. K. Topaloglu, J. A. Tello, L. D. Kotan, M. N. Ozbek, M. B. Yilmaz, S. Erdogan, F. Gurbuz, F. Temiz, R. P. Millar, B. Yuksel, Inactivating KISS1 mutation and hypogonadotropic hypogonadism. *N Engl J Med* **366**, 629-635 (2012); published online EpubFeb 16 (10.1056/NEJMoa1111184).

14.   S. B. Seminara, S. Messager, E. E. Chatzidaki, R. R. Thresher, J. S. Acierno, Jr., J. K. Shagoury, Y. Bo-Abbas, W. Kuohung, K. M. Schwinof, A. G. Hendrick, D. Zahn, J. Dixon, U. B. Kaiser, S. A. Slaugenhaupt, J. F. Gusella, S. O'Rahilly, M. B. Carlton, W. F. Crowley, Jr., S. A. Aparicio, W. H. Colledge, The GPR54 gene as a regulator of puberty. *N.Engl.J.Med.* **349**, 1614-1627 (2003).

15.   N. de Roux, E. Genin, J. C. Carel, F. Matsuda, J. L. Chaussain, E. Milgrom, Hypogonadotropic hypogonadism due to loss of function of the KiSS1-derived peptide receptor GPR54. *Proc.Natl.Acad.Sci.U.S.A* **100**, 10972-10976 (2003).

16.   S. Constantin, D. Reynolds, A. Oh, K. Pizano, S. Wray, Nitric oxide resets kisspeptin-excited GnRH neurons via PIP2 replenishment. *Proc Natl Acad Sci U S A* **118**, (2021); published online EpubJan 5 (10.1073/pnas.2012339118).

17.   K. Chachlaki, S. A. Malone, E. Qualls-Creekmore, E. Hrabovszky, H. Munzberg, P. Giacobini, F. Ango, V. Prevot, Phenotyping of nNOS neurons in the postnatal and adult female mouse hypothalamus. *J Comp Neurol* **525**, 3177-3189 (2017); published online EpubOct 15 (10.1002/cne.24257).

18.   N. K. Hanchate, J. Parkash, N. Bellefontaine, D. Mazur, W. H. Colledge, X. d'Anglemont de Tassigny, V. Prevot, Kisspeptin-GPR54 Signaling in Mouse

24

616 NO-Synthesizing Neurons Participates in the Hypothalamic Control of Ovulation. *J Neurosci* **32**, 932-945 (2012); published online EpubJan 18 (32/3/932 [pii]

618 10.1523/JNEUROSCI.4765-11.2012).

19. S. Mandal, A. Stanco, E. S. Buys, G. Enikolopov, J. L. Rubenstein, Soluble
620 guanylate cyclase generation of cGMP regulates migration of MGE neurons. *J Neurosci* **33**, 16897-16914 (2013); published online EpubOct 23
622 (10.1523/JNEUROSCI.1871-13.2013).

20. C. Charriaut-Marlangue, P. Bonnin, H. Pham, G. Loron, P. L. Leger, P.
624 Gressens, S. Renolleau, O. Baud, Nitric oxide signaling in the brain: a new target for inhaled nitric oxide? *Ann Neurol* **73**, 442-448 (2013); published
626 online EpubApr (10.1002/ana.23842).

21. K. Chachlaki, J. Garthwaite, V. Prevot, The gentle art of saying NO: how nitric
628 oxide gets things done in the hypothalamus. *Nat Rev Endocrinol* **13**, 521-535 (2017); published online EpubSep (10.1038/nrendo.2017.69).

630 22. R. Gyurko, S. Leupen, P. L. Huang, Deletion of exon 6 of the neuronal nitric oxide synthase gene in mice results in hypogonadism and infertility.
632 *Endocrinology* **143**, 2767-2774 (2002).

23. M. A. Mittelman-Smith, H. Williams, S. J. Krajewski-Hall, J. Lai, P. Ciofi, N.
634 T. McMullen, N. E. Rance, Arcuate kisspeptin/neurokinin B/dynorphin (KNDy) neurons mediate the estrogen suppression of gonadotropin secretion
636 and body weight. *Endocrinology* **153**, 2800-2812 (2012); published online EpubJun (10.1210/en.2012-1045).

638 24. K. Chachlaki, V. Prevot, Nitric oxide signalling in the brain and its control of bodily functions. *Br J Pharmacol* **177**, 5437-5458 (2020); published online
640 EpubJul 26 (10.1111/bph.14800).

25. J. Harrington, M. R. Palmert, Clinical review: Distinguishing constitutional
642 delay of growth and puberty from isolated hypogonadotropic hypogonadism: critical appraisal of available diagnostic tests. *J Clin Endocrinol Metab* **97**,
644 3056-3067 (2012); published online EpubSep (10.1210/jc.2012-1598).

26. D. J. Stuehr, Structure-function aspects in the nitric oxide synthases. *Annu Rev*
646 *Pharmacol Toxicol* **37**, 339-359 (1997)10.1146/annurev.pharmtox.37.1.339).

27. Y. T. Phung, S. M. Black, Use of chimeric forms of neuronal nitric-oxide
648 synthase as dominant negative mutants. *IUBMB Life* **48**, 333-338 (1999); published online EpubSep (10.1080/713803520).

650 28. P. L. Huang, T. M. Dawson, D. S. Bredt, S. H. Snyder, M. C. Fishman, Targeted disruption of the neuronal nitric oxide synthase gene. *Cell* **75**, 1273-1286
652 (1993); published online EpubDec 31 (

29. F. Casoni, S. A. Malone, M. Belle, F. Luzzati, F. Collier, C. Allet, E.
654 Hrabovszky, S. Rasika, V. Prevot, A. Chedotal, P. Giacobini, Development of the neurons controlling fertility in humans: new insights from 3D imaging and
656 transparent fetal brains. *Development* **143**, 3969-3981 (2016); published online EpubNov 1 (10.1242/dev.139444).

658 30. M. Kavsek, M. H. Bornstein, Visual habituation and dishabituation in preterm infants: a review and meta-analysis. *Res Dev Disabil* **31**, 951-975 (2010);
660 published online EpubSep-Oct (10.1016/j.ridd.2010.04.016).

31. P. S. Kaplan, J. S. Werner, Habituation, response to novelty, and dishabituation
662 in human infants: tests of a dual-process theory of visual attention. *J Exp Child Psychol* **42**, 199-217 (1986); published online EpubOct (

664   32.   D. S. Tait, E. A. Chase, V. J. Brown, Attentional set-shifting in rodents: a review of behavioural methods and pharmacological results. *Curr Pharm Des*
666   **20**, 5046-5059 (2014)10.2174/1381612819666131216115802).

33.   V. J. Brown, D. S. Tait, Attentional Set-Shifting Across Species. *Curr Top*
668   *Behav Neurosci* **28**, 363-395 (2016)10.1007/7854_2015_5002).

34.   J. F. Keeler, T. W. Robbins, Translating cognition from animals to humans.
670   *Biochem Pharmacol* **81**, 1356-1366 (2011); published online EpubJun 15 (10.1016/j.bcp.2010.12.028).

672   35.   V. Prevot, in *Knobil and Neill's Physiology of Reproduction,* T. M. Plant, J. Zeleznik, Eds. (Elsevier, New York, 2015), pp. pp 1395-1439.

674   36.   J. Parkash, X. d'Anglemont de Tassigny, N. Bellefontaine, C. Campagne, D. Mazure, V. Buee-Scherrer, V. Prevot, Phosphorylation of N-methyl-D-aspartic
676   acid receptor-associated neuronal nitric oxide synthase depends on estrogens and modulates hypothalamic nitric oxide production during the ovarian cycle.
678   *Endocrinology* **151**, 2723-2735 (2010); published online EpubJun (

37.   T. R. Kumar, Y. Wang, N. Lu, M. M. Matzuk, Follicle stimulating hormone is
680   required for ovarian follicle maturation but not male fertility. *Nat Genet* **15**, 201-204 (1997); published online EpubFeb (10.1038/ng0297-201).

682   38.   J. Clasadonte, P. Poulain, J. C. Beauvillain, V. Prevot, Activation of neuronal nitric oxide release inhibits spontaneous firing in adult gonadotropin-releasing
684   hormone neurons: a possible local synchronizing signal. *Endocrinology* **149**, 587-596 (2008).

686   39.   D. D. Belsham, P. L. Mellon, Transcription factors Oct-1 and C/EBPbeta (CCAAT/enhancer-binding protein-beta) are involved in the glutamate/nitric
688   oxide/cyclic-guanosine 5'-monophosphate-mediated repression of mediated repression of gonadotropin-releasing hormone gene expression. *Mol*
690   *Endocrinol* **14**, 212-228 (2000); published online EpubFeb (

40.   S. Lakshminrusimha, B. Mathew, C. L. Leach, Pharmacologic strategies in
692   neonatal pulmonary hypertension other than nitric oxide. *Semin Perinatol* **40**, 160-173 (2016); published online EpubApr (10.1053/j.semperi.2015.12.004).

694   41.   T. J. Hayeck, N. Stong, C. J. Wolock, B. Copeland, S. Kamalakaran, D. B. Goldstein, A. S. Allen, Improved Pathogenic Variant Localization via a
696   Hierarchical Model of Sub-regional Intolerance. *Am J Hum Genet* **104**, 299-309 (2019); published online EpubFeb 7 (10.1016/j.ajhg.2018.12.020).

698   42.   J. Young, C. Xu, G. E. Papadakis, J. S. Acierno, L. Maione, J. Hietamaki, T. Raivio, N. Pitteloud, Clinical Management of Congenital Hypogonadotropic
700   Hypogonadism. *Endocr Rev* **40**, 669-710 (2019); published online EpubApr 1 (10.1210/er.2018-00116).

702   43.   M. J. Eliasson, S. Blackshaw, M. J. Schell, S. H. Snyder, Neuronal nitric oxide synthase alternatively spliced forms: prominent functional localizations in the
704   brain. *Proc.Natl.Acad.Sci.U.S.A* **94**, 3396-3401 (1997).

44.   R. Quinton, Y. Mamoojee, C. N. Jayasena, J. Young, S. Howard, L. Dunkel, T.
706   Cheetham, N. Smith, A. A. Dwyer, Society for Endocrinology UK guidance on the evaluation of suspected disorders of sexual development: emphasizing the
708   opportunity to predict adolescent pubertal failure through a neonatal diagnosis of absent minipuberty. *Clin Endocrinol (Oxf)* **86**, 305-306 (2017); published
710   online EpubFeb (10.1111/cen.13257).

45.   T. Kuiri-Hanninen, S. Kallio, R. Seuri, E. Tyrvainen, A. Liakka, J. Tapanainen,
712   U. Sankilampi, L. Dunkel, Postnatal developmental changes in the pituitary-

ovarian axis in preterm and term infant girls. *J Clin Endocrinol Metab* **96**, 3432-3439 (2011); published online EpubNov (10.1210/jc.2011-1502).

46.   T. Kuiri-Hanninen, R. Seuri, E. Tyrvainen, U. Turpeinen, E. Hamalainen, U. H. Stenman, L. Dunkel, U. Sankilampi, Increased activity of the hypothalamic-pituitary-testicular axis in infancy results in increased androgen action in premature boys. *J Clin Endocrinol Metab* **96**, 98-105 (2011); published online EpubJan (10.1210/jc.2010-1359).

47.   M. Garcia-Duran, T. de Frutos, J. Diaz-Recasens, G. Garcia-Galvez, A. Jimenez, M. Monton, J. Farre, L. Sanchez de Miguel, F. Gonzalez-Fernandez, M. D. Arriero, L. Rico, R. Garcia, S. Casado, A. Lopez-Farre, Estrogen stimulates neuronal nitric oxide synthase protein expression in human neutrophils. *Circ Res* **85**, 1020-1026 (1999); published online EpubNov 26 (

48.   X. d'Anglemont de Tassigny, C. Campagne, S. Steculorum, V. Prevot, Estradiol induces physical association of neuronal nitric oxide synthase with NMDA receptor and promotes nitric oxide formation via estrogen receptor activation in primary neuronal cultures. *J Neurochem* **109**, 214-224 (2009); published online EpubApr (

49.   X. d'Anglemont de Tassigny, C. Campagne, B. Dehouck, D. Leroy, G. R. Holstein, J. C. Beauvillain, V. Buee-Scherrer, V. Prevot, Coupling of neuronal nitric oxide synthase to NMDA receptors via postsynaptic density-95 depends on estrogen and contributes to the central control of adult female reproduction. *J Neurosci* **27**, 6103-6114 (2007); published online EpubJun 6 (27/23/6103 [pii]
10.1523/JNEUROSCI.5595-06.2007).

50.   M. M. McCarthy, Estradiol and the developing brain. *Physiol Rev* **88**, 91-124 (2008); published online EpubJan (

51.   B. McEwen, Estrogen actions throughout the brain. *Recent Prog Horm Res* **57**, 357-384 (2002).

52.   M. C. S. Denley, N. J. F. Gatford, K. J. Sellers, D. P. Srivastava, Estradiol and the Development of the Cerebral Cortex: An Unexpected Role? *Front Neurosci* **12**, 245 (2018)10.3389/fnins.2018.00245).

53.   E. Carosa, P. Martini, F. Brandetti, S. M. Di Stasi, F. Lombardo, A. Lenzi, E. A. Jannini, Type V phosphodiesterase inhibitor treatments for erectile dysfunction increase testosterone levels. *Clin Endocrinol (Oxf)* **61**, 382-386 (2004); published online EpubSep (10.1111/j.1365-2265.2004.02108.x).

54.   T. Raivio, J. Falardeau, A. Dwyer, R. Quinton, F. J. Hayes, V. A. Hughes, L. W. Cole, S. H. Pearce, H. Lee, P. Boepple, W. F. Crowley, Jr., N. Pitteloud, Reversal of idiopathic hypogonadotropic hypogonadism. *N Engl J Med* **357**, 863-873 (2007); published online EpubAug 30 (10.1056/NEJMoa066494).

55.   J. R. Steinert, S. W. Robinson, H. Tong, M. D. Haustein, C. Kopp-Scheinpflug, I. D. Forsythe, Nitric oxide is an activity-dependent regulator of target neuron intrinsic excitability. *Neuron* **71**, 291-305 (2011); published online EpubJul 28 (10.1016/j.neuron.2011.05.037).

56.   R. Weitzdoerfer, H. Hoeger, E. Engidawork, M. Engelmann, N. Singewald, G. Lubec, B. Lubec, Neuronal nitric oxide synthase knock-out mice show impaired cognitive performance. *Nitric Oxide* **10**, 130-140 (2004); published online EpubMay (10.1016/j.niox.2004.03.007).

57.   Y. Gao, S. A. Heldt, Lack of neuronal nitric oxide synthase results in attention deficit hyperactivity disorder-like behaviors in mice. *Behav Neurosci* **129**, 50-61 (2015); published online EpubFeb (10.1037/bne0000031).

58. C. M. Francois, F. Petit, F. Giton, A. Gougeon, C. Ravel, S. Magre, J. Cohen-Tannoudji, C. J. Guigon, A novel action of follicle-stimulating hormone in the ovary promotes estradiol production without inducing excessive follicular growth before puberty. *Sci Rep* **7**, 46222 (2017); published online EpubApr 11 (10.1038/srep46222).

59. L. Teixeira, F. Guimiot, C. Dode, C. Fallet-Bianco, R. P. Millar, A. L. Delezoide, J. P. Hardelin, Defective migration of neuroendocrine GnRH cells in human arrhinencephalic conditions. *J Clin Invest* **120**, 3668-3672 (2010); published online EpubOct 1 (

60. N. K. Hanchate, P. Giacobini, P. Lhuillier, J. Parkash, C. Espy, C. Fouveaut, C. Leroy, S. Baron, C. Campagne, C. Vanacker, F. Collier, C. Cruaud, V. Meyer, A. Garcia-Pinero, D. Dewailly, C. Cortet-Rudelli, K. Gersak, C. Metz, G. Chabrier, M. Pugeat, J. Young, J. P. Hardelin, V. Prevot, C. Dode, SEMA3A, a Gene Involved in Axonal Pathfinding, Is Mutated in Patients with Kallmann Syndrome. *PLoS Genet* **8**, e1002896 (2012); published online EpubAug (10.1371/journal.pgen.1002896

PGENETICS-D-12-00582 [pii]).

61. H. Song, G. Ming, Z. He, M. Lehmann, L. McKerracher, M. Tessier-Lavigne, M. Poo, Conversion of neuronal growth cone responses from repulsion to attraction by cyclic nucleotides. *Science* **281**, 1515-1518 (1998); published online EpubSep 4 (

62. C. Vanacker, S. Trova, S. Shruti, F. Casoni, A. Messina, S. Croizier, S. Malone, G. Ternier, N. K. Hanchate, S. Rasika, S. G. Bouret, P. Ciofi, P. Giacobini, V. Prevot, Neuropilin-1 expression in GnRH neurons regulates prepubertal weight gain and sexual attraction. *EMBO J* **39**, e104633 (2020); published online EpubOct 1 (10.15252/embj.2020104633).

63. M. Pietrobon, I. Zamparo, M. Maritan, S. A. Franchi, T. Pozzan, C. Lodovichi, Interplay among cGMP, cAMP, and Ca2+ in living olfactory sensory neurons in vitro and in vivo. *J Neurosci* **31**, 8395-8405 (2011); published online EpubJun 8 (10.1523/JNEUROSCI.6722-10.2011).

64. S. Watanabe, F. Takanashi, K. Ishida, S. Kobayashi, Y. Kitamura, Y. Hamasaki, M. Saito, Nitric Oxide-Mediated Modulation of Central Network Dynamics during Olfactory Perception. *PLoS One* **10**, e0136846 (2015)10.1371/journal.pone.0136846).

65. S. Fujie, H. Aonuma, I. Ito, A. Gelperin, E. Ito, The nitric oxide/cyclic GMP pathway in the olfactory processing system of the terrestrial slug Limax marginatus. *Zoolog Sci* **19**, 15-26 (2002); published online EpubJan (10.2108/zsj.19.15).

66. K. M. Kendrick, R. Guevara-Guzman, J. Zorrilla, M. R. Hinton, K. D. Broad, M. Mimmack, S. Ohkura, Formation of olfactory memories mediated by nitric oxide. *Nature* **388**, 670-674 (1997); published online EpubAug 14 (10.1038/41765).

67. C. H. Wilson, T. A. Christensen, A. J. Nighorn, Inhibition of nitric oxide and soluble guanylyl cyclase signaling affects olfactory neuron activity in the moth, Manduca sexta. *J Comp Physiol A Neuroethol Sens Neural Behav Physiol* **193**, 715-728 (2007); published online EpubJul (10.1007/s00359-007-0227-9).

68. D. A. Hopkins, H. W. Steinbusch, M. Markerink-van Ittersum, J. De Vente, Nitric oxide synthase, cGMP, and NO-mediated cGMP production in the olfactory bulb of the rat. *J Comp Neurol* **375**, 641-658 (1996); published online

812 EpubNov 25 (10.1002/(SICI)1096-9861(19961125)375:4<641::AID-CNE6>3.0.CO;2-1).

814 69. L. Sulz, G. Astorga, B. Bellette, R. Iturriaga, A. Mackay-Sim, J. Bacigalupo, Nitric oxide regulates neurogenesis in adult olfactory epithelium in vitro. *Nitric Oxide* **20**, 238-252 (2009); published online EpubJun (10.1016/j.niox.2009.01.004).

818 70. C. Cserep, A. Szonyi, J. M. Veres, B. Nemeth, E. Szabadits, J. de Vente, N. Hajos, T. F. Freund, G. Nyiri, Nitric oxide signaling modulates synaptic transmission during early postnatal development. *Cereb Cortex* **21**, 2065-2074 (2011); published online EpubSep (10.1093/cercor/bhq281).

822 71. G. J. Qu, J. Ma, Y. C. Yu, Y. Fu, Postnatal development of GABAergic interneurons in the neocortical subplate of mice. *Neuroscience* **322**, 78-93 (2016); published online EpubMay 13 (10.1016/j.neuroscience.2016.02.023).

72. K. Y. Kwan, M. M. Lam, M. B. Johnson, U. Dube, S. Shim, M. R. Rasin, A. M. Sousa, S. Fertuzinhos, J. G. Chen, J. I. Arellano, D. W. Chan, M. Pletikos, L. Vasung, D. H. Rowitch, E. J. Huang, M. L. Schwartz, R. Willemsen, B. A. Oostra, P. Rakic, M. Heffer, I. Kostovic, M. Judas, N. Sestan, Species-dependent posttranscriptional regulation of NOS1 by FMRP in the developing cerebral cortex. *Cell* **149**, 899-911 (2012); published online EpubMay 11 (10.1016/j.cell.2012.02.060).

832 73. A. J. Roskams, D. S. Bredt, T. M. Dawson, G. V. Ronnett, Nitric oxide mediates the formation of synaptic connections in developing and regenerating olfactory receptor neurons. *Neuron* **13**, 289-299 (1994); published online EpubAug (

74. M. R. Bowl, S. J. Dawson, Age-Related Hearing Loss. *Cold Spring Harb Perspect Med*, (2018); published online EpubOct 5 (10.1101/cshperspect.a033217).

838 75. J. Shen, D. I. Scheffer, K. Y. Kwan, D. P. Corey, SHIELD: an integrative gene expression database for inner ear research. *Database (Oxford)* **2015**, bav071 (2015)10.1093/database/bav071).

76. D. Mohrle, K. Reimann, S. Wolter, M. Wolters, K. Varakina, E. Mergia, N. Eichert, H. S. Geisler, P. Sandner, P. Ruth, A. Friebe, R. Feil, U. Zimmermann, D. Koesling, M. Knipper, L. Ruttiger, NO-Sensitive Guanylate Cyclase Isoforms NO-GC1 and NO-GC2 Contribute to Noise-Induced Inner Hair Cell Synaptopathy. *Mol Pharmacol* **92**, 375-388 (2017); published online EpubOct (10.1124/mol.117.108548).

77. B. M. J. Olthof, S. E. Gartside, A. Rees, Puncta of Neuronal Nitric Oxide Synthase (nNOS) Mediate NMDA Receptor Signaling in the Auditory Midbrain. *J Neurosci* **39**, 876-887 (2019); published online EpubJan 30 (10.1523/JNEUROSCI.1918-18.2018).

78. A. Reif, C. P. Jacob, D. Rujescu, S. Herterich, S. Lang, L. Gutknecht, C. G. Baehne, A. Strobel, C. M. Freitag, I. Giegling, M. Romanos, A. Hartmann, M. Rosler, T. J. Renner, A. J. Fallgatter, W. Retz, A. C. Ehlis, K. P. Lesch, Influence of functional variant of neuronal nitric oxide synthase on impulsive behaviors in humans. *Arch Gen Psychiatry* **66**, 41-50 (2009); published online EpubJan (10.1001/archgenpsychiatry.2008.510).

79. G. K. Swamy, T. Ostbye, R. Skjaerven, Association of preterm birth with long-term survival, reproduction, and next-generation preterm birth. *JAMA* **299**, 1429-1436 (2008); published online EpubMar 26 (10.1001/jama.299.12.1429).

860 80. B. M. D'Onofrio, Q. A. Class, M. E. Rickert, H. Larsson, N. Langstrom, P. Lichtenstein, Preterm birth and mortality and morbidity: a population-based

862   quasi-experimental study. *JAMA Psychiatry* **70**, 1231-1240 (2013); published online EpubNov (10.1001/jamapsychiatry.2013.2107).

864 81.   D. Moster, R. T. Lie, T. Markestad, Long-term medical and social consequences of preterm birth. *N Engl J Med* **359**, 262-273 (2008); published
866   online EpubJul 17 (10.1056/NEJMoa0706475).

82.   H. M. Lewkowitz-Shpuntoff, V. A. Hughes, L. Plummer, M. G. Au, R. L. Doty,
868   S. B. Seminara, Y. M. Chan, N. Pitteloud, W. F. Crowley, Jr., R. Balasubramanian, Olfactory phenotypic spectrum in idiopathic
870   hypogonadotropic hypogonadism: pathophysiological and genetic implications. *The Journal of clinical endocrinology and metabolism* **97**, E136-
872   144 (2012); published online EpubJan (10.1210/jc.2011-2041).

83.   H. Li, R. Durbin, Fast and accurate short read alignment with Burrows-Wheeler
874   transform. *Bioinformatics* **25**, 1754-1760 (2009); published online EpubJul 15 (10.1093/bioinformatics/btp324).

876 84.   M. A. DePristo, E. Banks, R. Poplin, K. V. Garimella, J. R. Maguire, C. Hartl, A. A. Philippakis, G. del Angel, M. A. Rivas, M. Hanna, A. McKenna, T. J.
878   Fennell, A. M. Kernytsky, A. Y. Sivachenko, K. Cibulskis, S. B. Gabriel, D. Altshuler, M. J. Daly, A framework for variation discovery and genotyping
880   using next-generation DNA sequencing data. *Nature genetics* **43**, 491-498 (2011); published online EpubMay (10.1038/ng.806).

882 85.   K. Wang, M. Li, H. Hakonarson, ANNOVAR: functional annotation of genetic variants from high-throughput sequencing data. *Nucleic Acids Res* **38**, e164
884   (2010); published online EpubSep (10.1093/nar/gkq603).

86.   X. Liu, X. Jian, E. Boerwinkle, dbNSFP v2.0: a database of human non-
886   synonymous SNVs and their functional predictions and annotations. *Human mutation* **34**, E2393-2402 (2013); published online EpubSep
888   (10.1002/humu.22376).

87.   M. Kircher, D. M. Witten, P. Jain, B. J. O'Roak, G. M. Cooper, J. Shendure, A
890   general framework for estimating the relative pathogenicity of human genetic variants. *Nat Genet* **46**, 310-315 (2014); published online EpubMar
892   (10.1038/ng.2892).

88.   Y. Bhargava, K. Hampden-Smith, K. Chachlaki, K. C. Wood, J. Vernon, C. K.
894   Allerston, A. M. Batchelor, J. Garthwaite, Improved genetically-encoded, FlincG-type fluorescent biosensors for neural cGMP imaging. *Front Mol*
896   *Neurosci* **6**, 26 (2013)10.3389/fnmol.2013.00026).

89.   L. G. L. Amato, L. R. Montenegro, A. M. Lerario, A. A. L. Jorge, G. Guerra
898   Junior, C. Schnoll, A. C. Renck, E. B. Trarbach, E. M. F. Costa, B. B. Mendonca, A. C. Latronico, L. F. G. Silveira, New genetic findings in a large
900   cohort of congenital hypogonadotropic hypogonadism. *Eur J Endocrinol* **181**, 103-119 (2019); published online EpubAug 1 (10.1530/EJE-18-0764).

902 90.   A. Messina, K. Pulli, S. Santini, J. Acierno, J. Kansakoski, D. Cassatella, C. Xu, F. Casoni, S. A. Malone, G. Ternier, D. Conte, Y. Sidis, J. Tommiska, K.
904   Vaaralahti, A. Dwyer, Y. Gothilf, G. R. Merlo, F. Santoni, N. J. Niederlander, P. Giacobini, T. Raivio, N. Pitteloud, Neuron-Derived Neurotrophic Factor Is
906   Mutated in Congenital Hypogonadotropic Hypogonadism. *Am J Hum Genet* **106**, 58-70 (2020); published online EpubJan 2 (10.1016/j.ajhg.2019.12.003).

908 91.   S. Richards, N. Aziz, S. Bale, D. Bick, S. Das, J. Gastier-Foster, W. W. Grody, M. Hegde, E. Lyon, E. Spector, K. Voelkerding, H. L. Rehm, A. L. Q. A.
910   Committee, Standards and guidelines for the interpretation of sequence variants: a joint consensus recommendation of the American College of

912   Medical Genetics and Genomics and the Association for Molecular Pathology. *Genet Med* **17**, 405-424 (2015); published online EpubMay

914   (10.1038/gim.2015.30).

92.   H. Tang, P. D. Thomas, PANTHER-PSEP: predicting disease-causing genetic

916   variants using position-specific evolutionary preservation. *Bioinformatics* **32**, 2230-2232 (2016); published online EpubJul 15

918   (10.1093/bioinformatics/btw222).

93.   H. Ashkenazy, S. Abadi, E. Martz, O. Chay, I. Mayrose, T. Pupko, N. Ben-Tal,

920   ConSurf 2016: an improved methodology to estimate and visualize evolutionary conservation in macromolecules. *Nucleic Acids Res* **44**, W344-

922   350 (2016); published online EpubJul 8 (10.1093/nar/gkw408).

94.   J. Goedhart, L. van Weeren, M. J. Adjobo-Hermans, I. Elzenaar, M. A. Hink,

924   T. W. Gadella, Jr., Quantitative co-expression of proteins at the single cell level--application to a multimeric FRET sensor. *PLoS One* **6**, e27321

926   (2011)10.1371/journal.pone.0027321).

95.   J. Garthwaite, E. Southam, C. L. Boulton, E. B. Nielsen, K. Schmidt, B. Mayer,

928   Potent and selective inhibition of nitric oxide-sensitive guanylyl cyclase by 1H-[1,2,4]oxadiazolo[4,3-a]quinoxalin-1-one. *Mol.Pharmacol.* **48**, 184-188

930   (1995).

96.   N. Bellefontaine, K. Chachlaki, J. Parkash, C. Vanacker, W. Colledge, X.

932   d'Anglemont de Tassigny, J. Garthwaite, S. G. Bouret, V. Prevot, Leptin-dependent neuronal NO signaling in the preoptic hypothalamus facilitates

934   reproduction. *J Clin Invest* **124**, 2550-2559 (2014); published online EpubJun 2 (10.1172/JCI65928

936 65928 [pii]).

97.   A. M. Batchelor, K. Bartus, C. Reynell, S. Constantinou, E. J. Halvey, K. F.

938   Held, W. R. Dostmann, J. Vernon, J. Garthwaite, Exquisite sensitivity to subsecond, picomolar nitric oxide transients conferred on cells by guanylyl

940   cyclase-coupled receptors. *Proc Natl Acad Sci U S A* **107**, 22060-22065 (2010); published online EpubDec 21 (10.1073/pnas.1013147107).

942 98.   D. J. Spergel, U. Kruth, D. F. Hanley, R. Sprengel, P. H. Seeburg, GABA- and glutamate-activated channels in green fluorescent protein-tagged

944   gonadotropin-releasing hormone neurons in transgenic mice. *J.Neurosci.* **19**, 2037-2050 (1999).

946 99.   F. J. Steyn, Y. Wan, J. Clarkson, J. D. Veldhuis, A. E. Herbison, C. Chen, Development of a methodology for and assessment of pulsatile luteinizing

948   hormone secretion in juvenile and adult male mice. *Endocrinology* **154**, 4939-4945 (2013); published online EpubDec (10.1210/en.2013-1502).

950 100.   H. Fonseca, S. K. Powers, D. Goncalves, A. Santos, M. P. Mota, J. A. Duarte, Physical inactivity is a major contributor to ovariectomy-induced sarcopenia.

952   *Int J Sports Med* **33**, 268-278 (2012); published online EpubApr (10.1055/s-0031-1297953).

954 101.   M. M. Devillers, F. Petit, V. Cluzet, C. M. Francois, F. Giton, G. Garrel, J. Cohen-Tannoudji, C. J. Guigon, FSH inhibits AMH to support ovarian estradiol

956   synthesis in infantile mice. *J Endocrinol* **240**, 215-228 (2019); published online EpubFeb 1 (10.1530/JOE-18-0313).

958 102.   J. Pansiot, G. Loron, P. Olivier, R. Fontaine, C. Charriaut-Marlangue, J. C. Mercier, P. Gressens, O. Baud, Neuroprotective effect of inhaled nitric oxide

960   on excitotoxic-induced brain damage in neonatal rat. *PLoS One* **5**, e10916 (2010); published online EpubJun 1 (10.1371/journal.pone.0010916).

962 103. T. Hua-Huy, S. Duong-Quy, H. Pham, J. Pansiot, J. C. Mercier, O. Baud, A. T. Dinh-Xuan, Inhaled nitric oxide decreases pulmonary endothelial nitric oxide
964 synthase expression and activity in normal newborn rat lungs. *ERJ Open Res* **2**, (2016); published online EpubJan (10.1183/23120541.00060-2015).

966 104. N. Ambalavanan, J. L. Aschner, Management of hypoxemic respiratory failure and pulmonary hypertension in preterm infants. *J Perinatol* **36 Suppl 2**, S20-
968 27 (2016); published online EpubJun (10.1038/jp.2016.45).

105. L. Fodoulian, O. Gschwend, C. Huber, S. Mutel, R. F. Salazar, R. Leone, J.-R.
970 Renfer, K. Ekundayo, I. Rodriguez, A. Carleton, The claustrum-medial prefrontal cortex network controls attentional set-shifting. *bioRxiv*,
972 (2020)10.1101/2020.10.14.339259).

106. K. Skrapits, B. A. Borsay, L. Herczeg, P. Ciofi, S. R. Bloom, M. A. Ghatei, W.
974 S. Dhillo, Z. Liposits, E. Hrabovszky, Colocalization of cocaine- and amphetamine-regulated transcript with kisspeptin and neurokinin B in the
976 human infundibular region. *PLoS One* **9**, e103977 (2014)10.1371/journal.pone.0103977).

978 107. E. Hrabovszky, C. S. Molnar, M. T. Sipos, B. Vida, P. Ciofi, B. A. Borsay, L. Sarkadi, L. Herczeg, S. R. Bloom, M. A. Ghatei, W. S. Dhillo, I. Kallo, Z.
980 Liposits, Sexual dimorphism of kisspeptin and neurokinin B immunoreactive neurons in the infundibular nucleus of aged men and women. *Front Endocrinol*
982 *(Lausanne)* **2**, 80 (2011)10.3389/fendo.2011.00080).

108. B. A. Borsay, K. Skrapits, L. Herczeg, P. Ciofi, S. R. Bloom, M. A. Ghatei, W.
984 S. Dhillo, Z. Liposits, E. Hrabovszky, Hypophysiotropic gonadotropin-releasing hormone projections are exposed to dense plexuses of kisspeptin,
986 neurokinin B and substance p immunoreactive fibers in the human: a study on tissues from postmenopausal women. *Neuroendocrinology* **100**, 141-152
988 (2014)10.1159/000368362).

109. L. W. Swanson, *Structure of the rat brain*. (Elsevier Science Publishers,
990 Amsterdam, 2004).

992

Acknowledgments

Author contributions: K.C. and V.P applied for funding, designed the preclinical study, analyzed data, prepared the figures, and wrote the manuscript along with N.P. and A.M. K.C., V.D. and V.L. designed and performed preclinical mouse studies. K.C., G.T. and P.G., studied GnRH neuronal migration in mice and human fetuses. N.P. designed the genetic approach in CHH patients and analyzed the data together with A.M., J.A., R.J., F.S., and K.C. G.P and X.C., collected patient data. M.K. performed *in silico* analyses. K.C., A.M., N.J.N, and V.D. validated mutations *in vitro*. CM., K.S. and E.H. designed and performed immunohistochemical analyses in the adult human hypothalamus. P.C. studied

NOS1 and NK3R expression in the arcuate nucleus of intact and gonadectomized mice.

1022 S.S. designed and performed electrophysiological analyses. P.A. and V.L. assessed auditory performances in mice. C.H. and A.C. performed the attentional set-shifting task

1024 in mice. M.T.S. assessed FSH and LH levels in mice. G.T. and P.G. developed the tissue clearing approaches. S.C.J. provided human fetuses and R.Q., M.N., D.L. D.P., M.D.,

1026 M.L.M., P.K. contributed patient data and material. K.C. and L.S. designed inhaled NO and sildenafil therapy in mice. K.C. and J.G. engineered the live NO/cGMP sensors. J.A.

1028 and S.R. edited the manuscript and all authors have contributed to the preparation of the manuscript.

1030 **Competing interests**: Authors declare no competing interests.

Data and materials availability: All the data associated with this study are present in the

1032 paper or supplementary materials. Request for materials should be addressed to Vincent Prevot or Nelly Pitteloud.

1034

34

Figure legends

1036
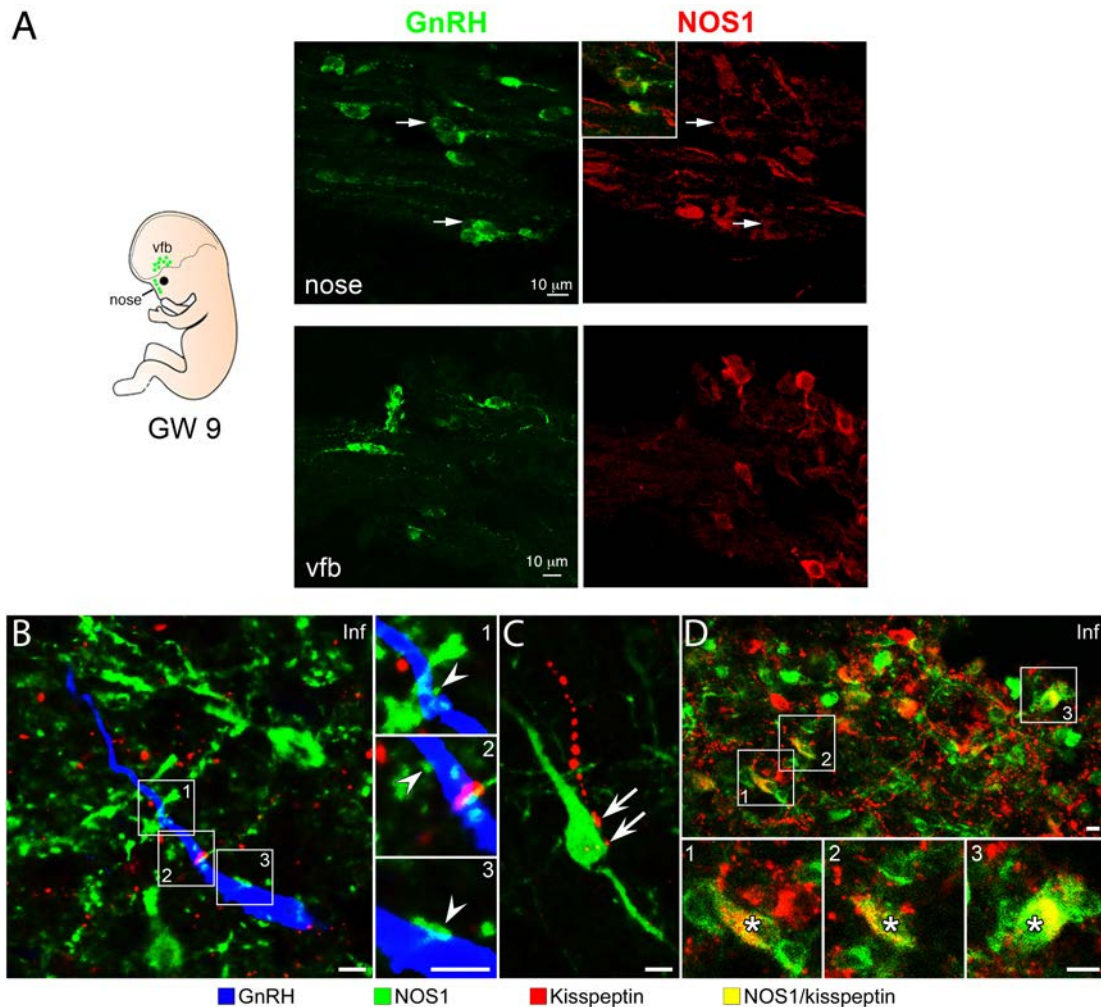
Figure 1. **NOS1 abundance in the GnRH neuronal system in humans**. (A) Immunolabeling of 9-weekold human fetuses reveals migrating GnRH neurons (green) co-expressing NOS1 protein (red), indicated by arrows, in the nose (upper panels), but not in the ventral forebrain (vfb; lower panels). (B) NOS1 (green), GnRH (blue) and kisspeptin (red) immunofluorescent staining in the infundibulum (Inf) of adult human hypothalami. Framed areas are shown at higher magnification in subpanels 1, 2 and 3. White arrowheads in subpanels 1 to 3 indicate contacts between NOS1-immunoreactive processes and GnRH-producing neurons. (C) Immunofluorescent staining of the infundibulum shows kisspeptin fibers (red) innervating (white arrows) NOS1-producing cells (green). (D) Immunofluorescent staining demonstrates a subpopulation (yellow, shown in subpanels 1 to 3) of kisspeptin neurons (asterisks) co-expressing NOS1 in the infundibulum. Scale bars: 15 µm in B to D.
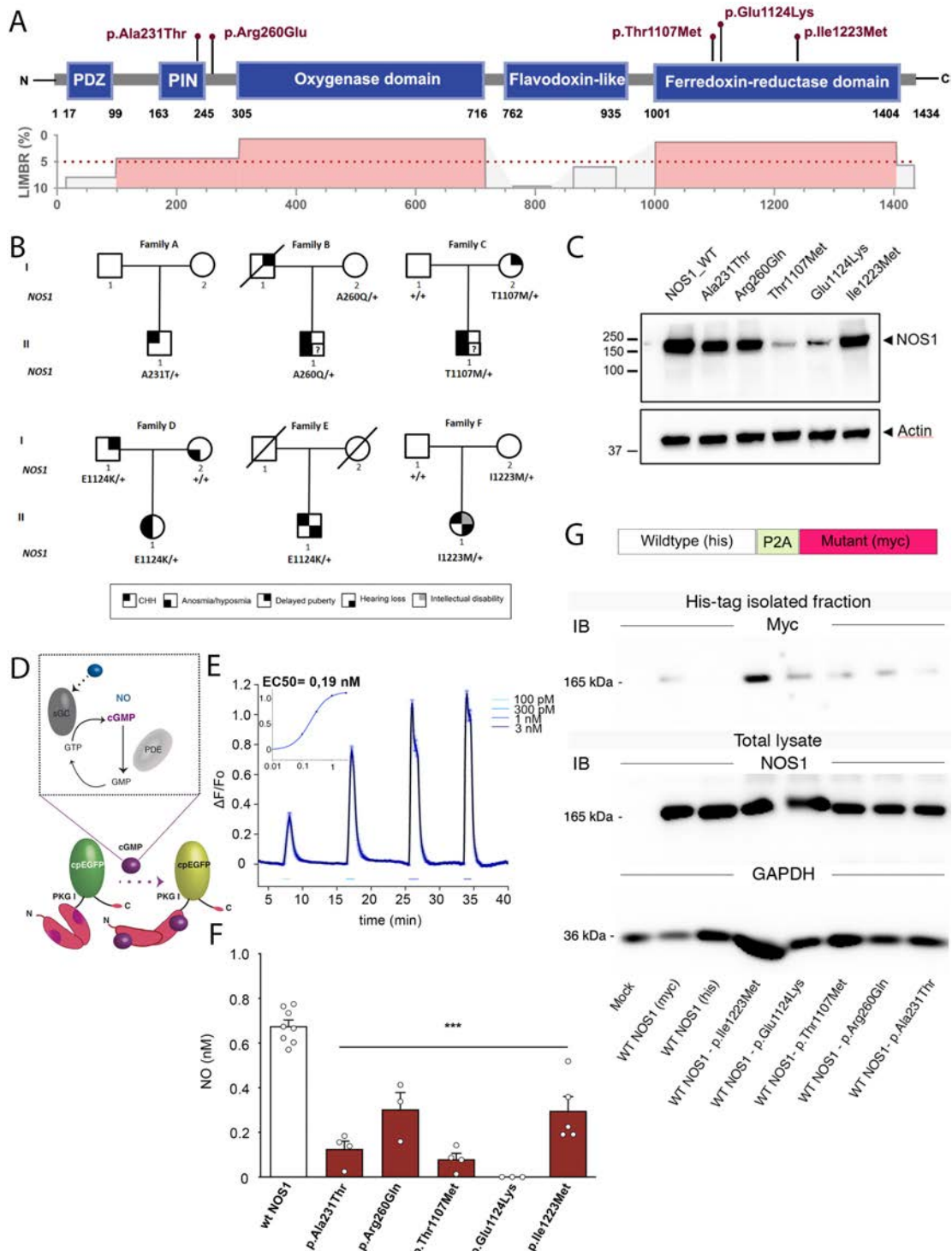
1050
**Figure 2**. **Identification and characterization of *NOS1* mutations in probands with**

1052 **CHH.** (A) Lollipop plot illustrating the distribution of identified mutations in functional
domains (blue boxes) of the human NOS1 protein (upper panel) and in highly constrained

1054 sub-regions (LIMBR score < 5%; lower panel in red). (B) Pedigrees of CHH probands
harboring *NOS1* mutations. Phenotypes are indicated by symbols as shown in the legend

1056 (bottom). (C) Representative western blot showing ectopic expression of NOS1 protein
(Anti-Myc tag) in HEK293 cells 48h after transfection with WT or mutant NOS1 constructs.

1058 (D) Mode of action of NO on the fluorometric probe (FlincG3) used to quantify NO

36

production from NOS1 isoforms using live-cell imaging in transfected HEKGC/PDE5 cells (that is, NO detector cells). sGC, soluble guanylate cyclase; PDE, phosphodiesterase; EGFP, enhanced green fluorescent protein. (E) Dose-response curve using increasing clamped applications of NO donor to calibrate the behavior of FlincG3-transfected HEKGC/PDE5 cells and calculate EC50 value and NO concentration (inset); F, fluorescence. (F) NO concentration upon endogenous stimulation of the NO signaling pathway in NO-detector cells expressing the WT or mutated NOS1 proteins (one-way ANOVA with Dunnett's post-hoc test; n=8,4,3,4,3,5). ***P<0.001. Values indicate means ± SEM. N>3 independent experiments using technical replicates. (G) Representative Western blots showing co-immunoprecipitation of Myc-tagged NOS1 mutants with His-tagged WT NOS1.
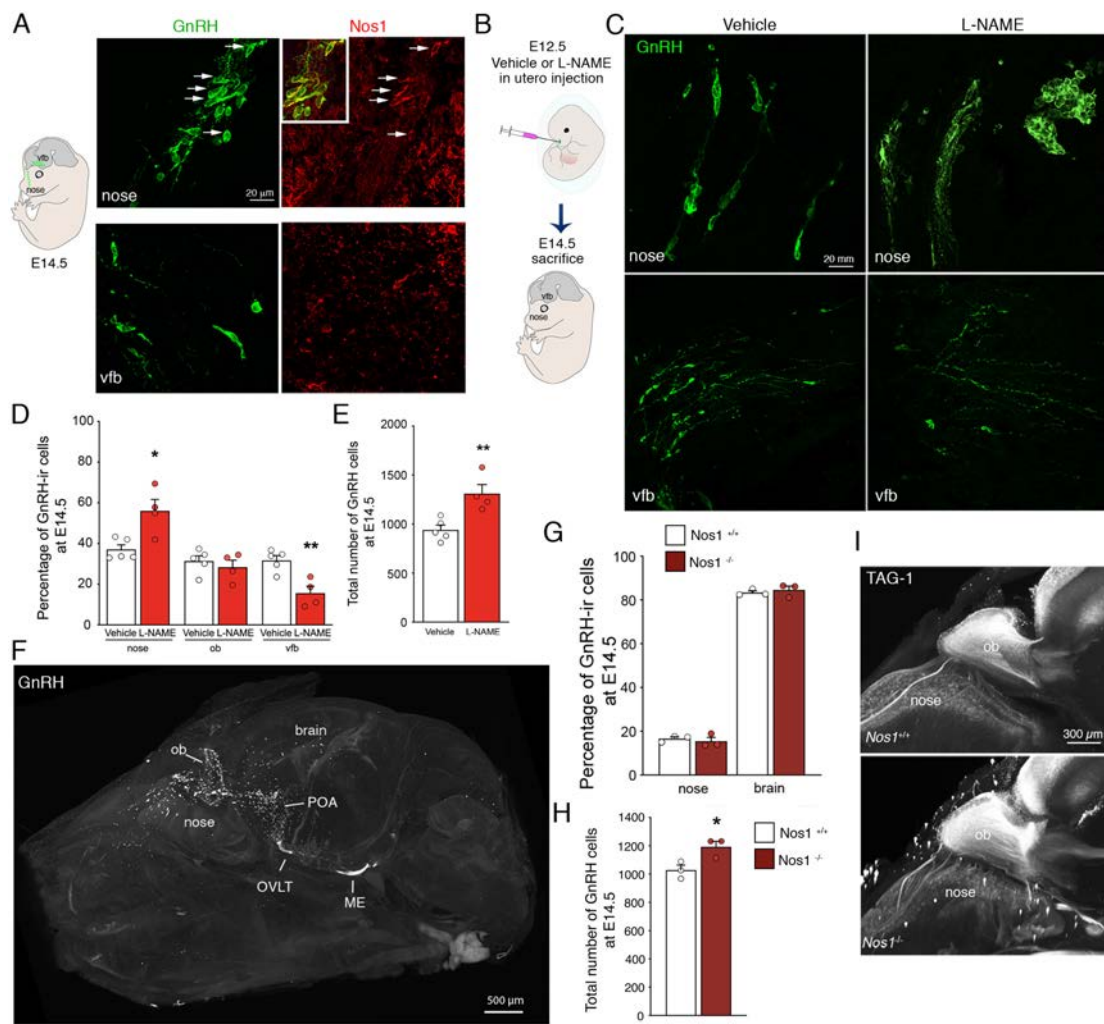
Figure 3. A role for Nos1 in GnRH neuron migration and number. (A) Immunolabeling of a mouse embryo on embryonic day 14.5 (E14.5) showing migrating GnRH-producing neurons (green) and Nos1 protein expression (red) in the nose (upper panels) and the ventral forebrain (vfb) (lower panels). Arrows indicate dual-labelled cells, a subpopulation of which is shown in the inset (yellow). (B) Schematic showing *in utero* injections of L-NAME into the nose of mouse embryos at E12. (C) Immunolabeling of a mouse embryo on E14.5 injected with vehicle (left panels) or L-NAME (right panels) showing migrating GnRH neurons (green) in the nose (upper panels) and the vfb (lower panels). (D) Distribution and (E) total number of GnRH-producing neurons at E14.5 in vehicle (white; *n*=5)- and L-NAME-treated (red; *n*=4) embryos in the nose, olfactory bulb (ob) and vfb. (F) Transparentized whole head and immunofluorescence for GnRH (white) in a *Nos1^{-/-}* mouse at P0. ME, median eminence; ob, olfactory bulb; OVLT, organum vasculosum laminae terminalis; POA, preoptic region. (G) Percentage (Kruskal-Wallis followed by Dunn's multiple comparisons), and (H) total number of the GnRH neurons in newborn *Nos1^{+/+}* (white; *n*=3)- and *Nos1^{-/-}* (brown; *n*=3) mice. (I) Representative 3D images of TAG-

38

1088   1 immunoreactive olfactory fibers projecting into the brain in *Nos1*$^{+/+}$ (top) and *Nos1*$^{-/-}$

(bottom) littermates at P0. Values indicate means ± SEM. *N*≥3 independent litters.

1090   Unpaired *t*-test, *P<0.05, **P<0.01.
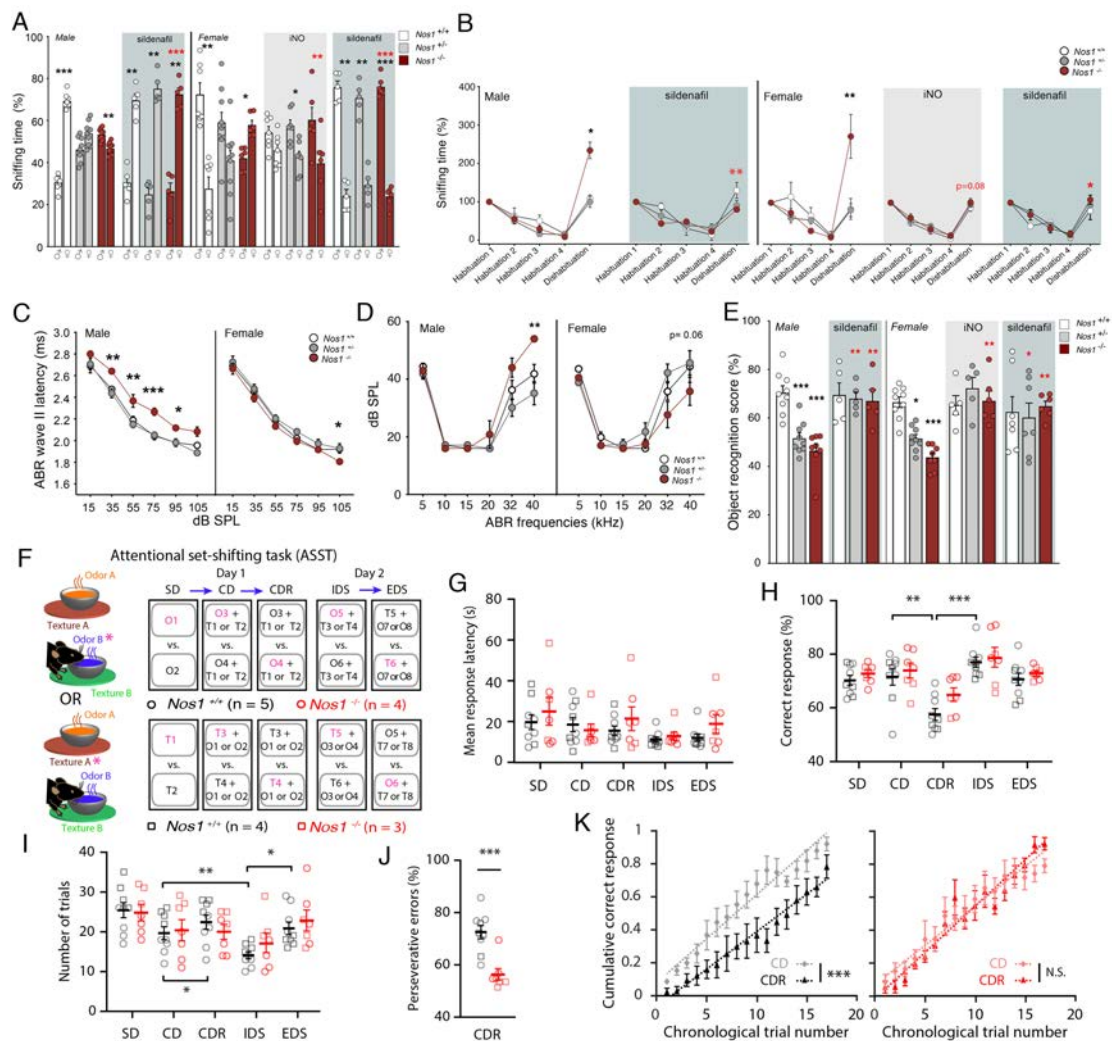
Figure 4. Behavioral tests for olfaction, cognition, and hearing in *Nos1*-deficient mice. (A) Social olfactory preference test in male and female *Nos1*[+/+](white), *Nos1*^{+/-} (grey) and *Nos1*^{-/-} mice (red) treated or not with iNO (grey-shaded area) or sildenafil (blue-shaded area) during the infantile period from P10 to P23. Black asterisks indicate the preference of each group for male versus female odor (paired *t*-test; males: untreated, *n*= 8,10,10; sildenafil-treated, *n*=5,5,5; females: untreated *n*=7,10,6; sildenafil-treated, *n*=5,5,6; iNO-treated, *n*=7,7,6). Red asterisks indicate the comparison between mice of the same sex and genotype but subjected to different treatments (*Nos1*^{-/-} females: Kruskal-Wallis followed by Dunn's multiple comparisons test; *Nos1*^{-/-} males: Mann-Whitney U test). (B) Non-social olfactory preference test in male and female *Nos1*[+/+](white), *Nos1*^{+/-} (grey) and *Nos1*^{-/-} mice (red) treated or not with iNO (grey-shaded area), or sildenafil (blue-shaded area) during the infantile period from P10 to P23. Values for *Nos1*^{+/+} mice during the dishabituation stage are compared to those of *Nos1*^{+/-} and *Nos1*^{-/-} mice for each treatment group [Kruskal-Wallis followed by Dunn's multiple comparisons test; males: untreated, *n*=6,5,5; sildenafil-treated, *n*=5,5,5; females: untreated, *n*=7,8,7; sildenafil-treated, *n*=

5,5,5; iNO-treated, *n*=6,5,6]. (C and D) Hearing assessed by measuring (C) latencies at the level of the cochlear nucleus (distortion-product otoacoustic emissions were identical in all mice), and (D) auditory brainstem-evoked response (ABR) thresholds in *Nos1*$^{+/+}$(white), *Nos1*$^{+/-}$ (grey) and *Nos1*$^{-/-}$ (red) male (*n*=8,8,6) and female mice (*n*=9,9,9). *Nos1*$^{+/+}$ values are compared to those of *Nos1*$^{+/-}$ and *Nos1*$^{-/-}$ mice for each group of measurements (two-way ANOVA with Dunnett's post-hoc test). (E) Recognition memory test in *Nos1*$^{+/+}$, *Nos1*$^{+/-}$ and *Nos1*$^{-/-}$ male and female mice treated or not (untreated males, *n*=9,9,8 and females, *n*=9,9,8) with iNO (grey-shaded area; females, *n*=6,5,6) or sildenafil (blue-shaded area; males, *n*=5,5,5; females, *n*=5,5,6) during the infantile period. *Nos1*$^{+/+}$ values are compared to those of *Nos1*$^{+/-}$ and *Nos1*$^{-/-}$ mice for each group of measurements (Kruskal-Wallis test with Dunn's post-hoc test). Red asterisks indicate the comparison between mice of the same genotype but subjected to different treatments (Mann-Whitney test for males and Kruskal-Wallis test with Dunn's post-hoc test for females). (F to K) Attentional-set formation and reversal learning in *Nos1*$^{+/+}$ (grey, *n*=9) and *Nos1*$^{-/-}$ male mice (red, *n*=7). (F) Schematics of the attentional set-shifting task (ASST). Mice performed simple discrimination (SD), compound discrimination (CD), reversal of CD (CDR) on day 1 and intradimentional set-shifting (IDS) and extradimentional set-shifting (EDS) on day 2. Half the mice started the task with olfactory cues being informative (top, pink O letters; these animals are shown with circles in panels G to H) whereas the other half started with tactile cues being informative (bottom, pink T letters, these animals are shown with squares in panels G to H) (see Materials and Methods for details). (G) Mean response latency during the ASST according to genotype (two-way repeated-measures ANOVA, *P*=0.6) and group (one-way repeated-measures ANOVA, *Nos1*$^{+/+}$[black]: *P*=0.12; *Nos1*$^{-/-}$ [red]: *P*=0.35). (H) Percentage of correctly completed trials according to genotype (two-way repeated-measures ANOVA, *P*=0.15) and group (one-way repeated-measures ANOVA, *Nos1*$^{+/+}$[black]: *P*=0.0002; *Nos1*$^{-/-}$[red]: *P*=0.015). (I) Number of trials performed for each block of the ASST according to genotype (two-way repeated-measures ANOVA, *P*=0.5327) and group (one-way repeated-measures ANOVA followed by post-hoc test including 5% false discovery rate, *Nos1*$^{+/+}$[black]: *P*=0.0028; *Nos1*$^{-/-}$[red]: *P*=0.21). (Number of trials done during the CDR block for *Nos1*$^{+/+}$ vs. *Nos1*$^{-/-}$ mice, paired *t*-test; *P*=0.78). (J) Percentage of perseverative errors during the CDR block (Mann-Whitney U test *P*=0.0007; *Nos1*$^{+/+}$: black, *Nos1*$^{-/-}$: red). (K) Comparison of normalized cumulative correct response rate as a function of the trial chronological order between the CD (grey and light red) and CDR block (black and red) in *Nos1*$^{+/+}$ (left panel) and *Nos1*$^{-/-}$ (right panel). Dotted lines indicate linear regressions (slope*: P*=0.055 and *P*=0.11, elevation: ***P<10-7 and *P*=0.39 for *Nos1*$^{+/+}$ and *Nos1*$^{-/-}$ mice, respectively). Values indicate means ± SEM. N>3 independent litters. *P<0.05; **P<0.01; ***P<0.001.
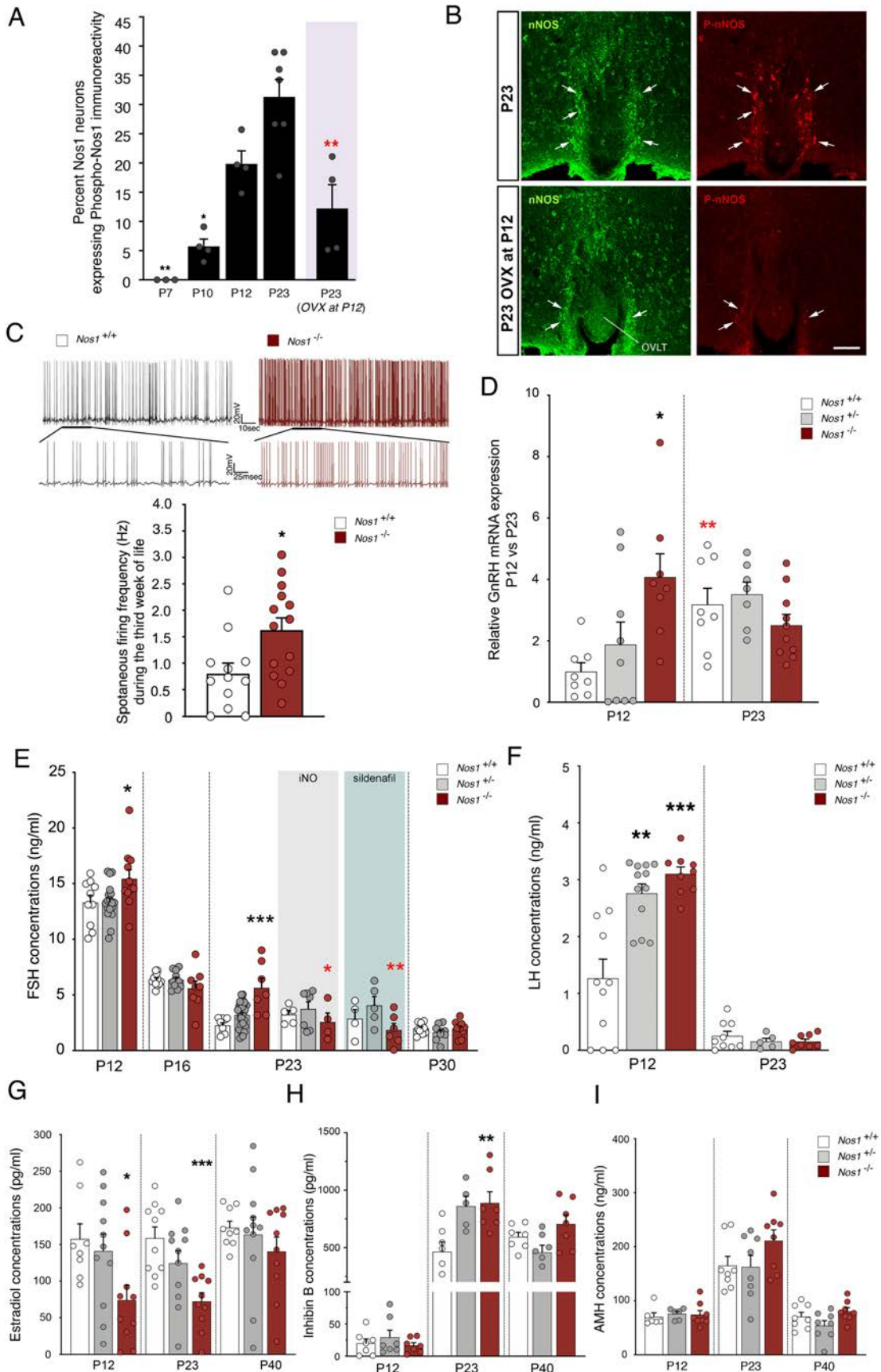
Figure 5. Nos1 activity controls infantile GnRH neuronal function. (A) Progressive

phosphorylation of Nos1 during postnatal development in the organum vasculosum

laminae terminalis (OVLT) in intact female mice and females ovariectomized (OVX) on postnatal day 12 (P12, grey-shaded area). Bar graphs represent the mean ratio of Nos1-immunoreactive pixels to P-Nos1-immunoreactive pixels. The abundance of P-Nos1 colocalization with NOS1 is compared across developmental stages for intact female mice (one-way ANOVA with Tukey's post-hoc test, n=3,4,4,7). The values for female mice after ovariectomy at P12 are independently compared to P23 values (unpaired t-test, n=7,4). (B) Immunolabeling for Nos1 (green) and p-Nos1 (red) at P23 in the OVLT of intact (upper panel) of ovariectomized female mice (OVX at P12; bottom panel) showing migrating GnRH neurons (green) and Nos1 protein expression (red). N>3 independent litters. Scale bar: 100 μm (applies to all panels). (C) Electrophysiological recordings of the spontaneous activity of preoptic area GnRH-producing neurons in late infantile (P14-P21) *Gnrh::Gfp; Nos1$^{+/+}$* and *Gnrh::Gfp; Nos1$^{-/-}$* bigenic mice. Upper panels show representative traces of spontaneous firing in a GnRH neuron from a *Nos1$^{+/+}$* (left panel, white) and a *Nos1$^{-/-}$* (right panel, red) animal. The bottom traces show an expansion of a small region of the top traces. The bottom panel displays quantification of spontaneous firing frequency in GnRH neurons from *Gnrh::Gfp; Nos1$^{+/+}$* and *Gnrh::Gfp; Nos1$^{-/-}$* mice (unpaired t-test, n=12,14 cells, N=5,6 mice). (D) RT-PCR analysis of *Gnrh* expression in FACS-isolated GnRH-GFP neurons from *Gnrh::Gfp; Nos1$^{+/+}$* (white), *Gnrh::Gfp; Nos1$^{+/-}$* (grey) and *Gnrh::Gfp; Nos1$^{-/-}$* bigenic mice (red) at P12 (n=8,9,8) and P23 (n=8,7,10). *Gnrh::Gfp; Nos1$^{+/+}$* values are compared to those of *Gnrh::Gfp; Nos1$^{+/-}$* and *Gnrh::Gfp; Nos1$^{-/-}$* mice (Kruskal-Wallis test with Dunn's post-hoc test at P12 and one-way ANOVA with Dunnett's post-hoc test at P23) * P < 0.05; ** P < 0.01. Red asterisks indicate the comparison between mice of the same genotype at P12 and P23 (Mann Whitney U test). (E) FSH concentrations at P12, P16, P23 and P30 in *Nos1$^{+/+}$* (white), *Nos1$^{+/-}$* (grey) and *Nos1$^{-/-}$* (red) female mice treated or not with iNO (grey-shaded area) or sildenafil (blue-shaded area) during the infantile period. FSH values for *Nos1$^{+/+}$* are compared to those of *Nos1$^{+/-}$* and *Nos1$^{-/-}$* mice for each group of measurements (one-way ANOVA with Dunnett's post-hoc test; P12: n=10,19,11; P16: n=11,11,8; P23: untreated, n=9,29,7; sildenafil-treated, n=4,5,6; iNO-treated, n=5,7,4; P30: n=10,9,10; Kruskal-Wallis test with Dunn's post-hoc test at P23). Red asterisks indicate the comparison between mice of the same genotype but subjected to different treatments (one-way ANOVA with Dunnett's post-hoc test). (F) LH concentrations at P12 (n=11,9,9) and P23 (n=12,5,8) in *Nos1$^{+/+}$* (white), *Nos1$^{+/-}$* (grey) and *Nos1$^{-/-}$* (red) female mice. *Nos1$^{+/+}$* LH values are compared to those of *Nos1$^{+/-}$* and *Nos1$^{-/-}$* mice for each age (P12: Kruskal-Wallis test with Dunn's post-hoc test; P23: one-way ANOVA with Dunnett's post-hoc test). *** P<0.001. Values indicate means ± SEM. N=4-8 independent litters. (G to I) Estradiol (G), inhibin B (H), and AMH (I) concentrations at P12, P23 and P40 in *Nos1$^{+/+}$* (white), *Nos1$^{+/-}$* (grey) and *Nos1$^{-/-}$* (red) female mice. P12: n=8,10,10 (G);

1186   *n*=7,7,7 (H); *n*=6,6,8 (I). P23: *n*=10,11,10 (G); *n*=7,5,7 (H); n=8,8,8 (I). P40: *n*=9,11,10 (G);

         n=7,7,7 (H); *n*=8,8,8 (I). $Nos1^{+/+}$ LH values are compared to those of $Nos1^{+/-}$ and $Nos1^{-/-}$

1188   mice for each group of measurements (G and H: one-way ANOVA with Dunnett's post-

         hoc test; I: Kruskal-Wallis test with Dunn's post-hoc test). Values indicate means ± SEM.

1190   N=3-8 independent litters. *P<0.05; **P<0.01; *** P<0.001.

1192
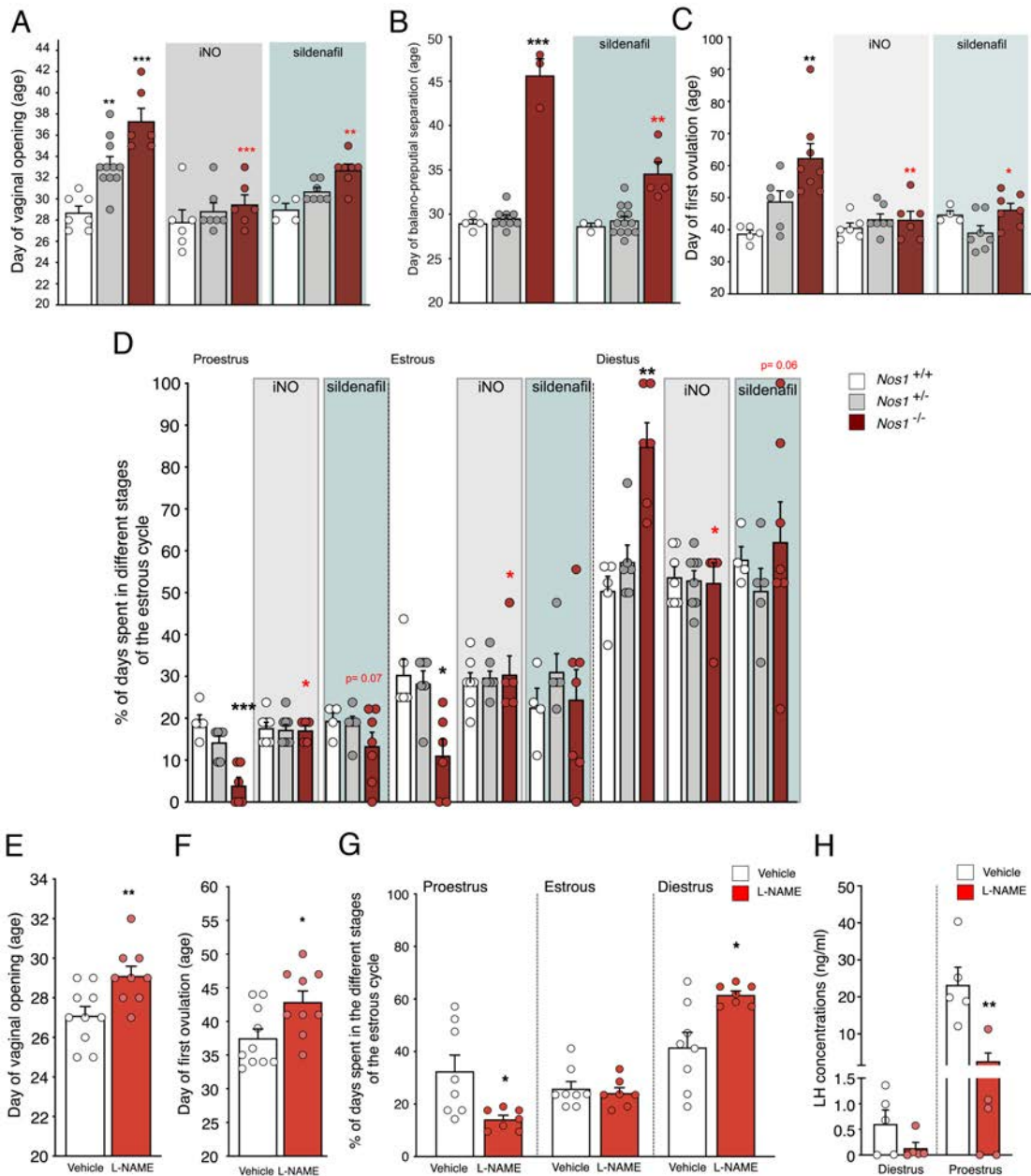
1194 **Figure 6. The action of NO during the critical infantile period is required for establishing a sexually mature phenotype.** (A) Age at vaginal opening in females, (B)
1196 balano-preputial separation in males (C) puberty in females and (D) adult estrous cyclicity in $Nos1^{+/+}$ (white), $Nos1^{+/-}$ (grey) and $Nos1^{-/-}$ (red) mice untreated (A: n=7,11,6; B: n=4,9,3;
1198 C: n=5,6,8; D: n=5,6,6) or treated with iNO (grey-shaded area, A: n=6,7,6; C: n=6,7,6; D: n=7,8,5) or sildenafil (blue-shaded area, A: n=4,7,7; B: n=3,13,5; C: n=4,7,7; D: n=4,5,7)
1200 during the infantile period. $Nos1^{+/+}$ values are compared to those of $Nos1^{+/-}$ and $Nos1^{-/-}$ mice for each group of measurements [one-way ANOVA with Dunnett's post-hoc test for
1202 a (untreated) or Kruskal-Wallis with Dunn's post-hoc test were used as detailed in Table S2. Red asterisks indicate a comparison between mice of the same genotype but

45

1204 subjected to different treatments (A: one-way ANOVA with Dunnett's post-hoc test, B: unpaired t-test; C,D: Kruskal-Wallis with Dunn's post-hoc test). (E to G) Age at vaginal

1206 opening (E) and puberty (F) (unpaired t-test; n=10,9), and adult estrous cyclicity (G) (Mann-Whitney U test; n=8,7) after daily injections of vehicle or L-NAME during the

1208 infantile period. (H) LH concentrations in diestrus and proestrus female mice subjected or not to LNAME treatment during the infantile period (Mann-Whitney U test; n=5,5). ** P =

1210 0.008. Values indicate means ± SEM. N>3 independent litters. *P<0.05; **P<0.01; *** P<0.001.

1212

1214

1216

1218

1220

1222

1224

1226

Table 1. **Genotype and clinical phenotype of six probands with ultra-rare heterozygous *NOS1* mutations**

Patient	Sex	*NOS1* mutations	rs number	MAF %	Diagnosis	Inheritance	Associated Phenotypes
A II-1	M	c.691G>A [p.Ala231Thr]	-	absent	nCHH	sporadic	-
B II-1	M	c.779G>A [p.Arg260Gln]	rs547371716	0.0019	KS	familial	supernumerary tooth
C II-1	M	c.3320C>T [p.Thr1107Met]	rs201943901	0.0064	KS	familial	bilateral cryptorchidism micropenis crowded teeth
D II-1	F	c.3370G>A [p.Glu1124Lys]	rs372660293	0.0055	KS	familial	scoliosis osteoporosis
E II-1	M	c.3370G>A [p.Glu1124Lys]	rs372660293	0.0055	nCHH	sporadic	**bilateral hearing loss** obesity
F II-1	F	c.3669A>G [p.Ile1223Met]	-	absent	nCHH	sporadic	**intellectual disability left hearing loss**

Nucleotide and protein changes are based on reference cDNA sequence NM_000620.4. Nucleotide and protein changes are based on reference cDNA sequence NM_000620.4. Abbreviations are as follows: MAF, minor-allele frequency in gnomAD exome controls; CHH, congenital hypogonadotropic hypogonadism; nCHH, normosmic CHH; KS, CHH with anosmia (Kallmann syndrome); M, male; F, female. Bold: associated phenotypes present in *Nos1*-deficient mice.

1230 # Supplementary Materials

1232 **This PDF file includes:**

1234   Supplementary Materials and Methods

      Figs. S1 to S7

1236   Tables S1 and S4

1238 **Other Supplementary Materials for this manuscript include the following:**

      Table S2 and Data file S1

1240

1242

MATERIALS AND METHODS

1244

Human tissues

1246 Human hypothalamic tissues were obtained at autopsies from the Forensic Medicine

Department of the University of Debrecen, Hungary, with the permission of the Regional

1248 Committee of Science and Research Ethics (DEOEC RKEB/IKEB: 3183-2010).

Permission to use 9 gestational-week-old human fetuses was obtained from the French

1250 Agence de Biomédecine (PFS16-002). Processing of human tissues and

immunochemistry protocols are detailed below.

1252

Genetic analyses

1254 Genomic DNA was extracted from peripheral blood samples using the Puregene Blood Kit

(Qiagen), following the manufacturer's protocol. Exome capture was performed using the

1256 SureSelect All Exon capture v2 or v5 (Agilent Technologies) and sequenced on the

HiSeq2500 (Illumina) at BGI (BGI, Shenzen). Raw sequences (FASTQ files) were

1258 analyzed using an in-house pipeline that utilizes the Burrows-Wheeler Alignment algorithm

(BWA) (*1*) for mapping the reads to the human reference sequence (GRCh37), and the

1260 Genome Analysis Toolkit (GATK) (*2*) for the detection of single nucleotide variants (SNVs)

and insertion/deletions (Indels). The resulting variants were annotated using Annovar

1262 version 20191024(*3*) and dbNSFP version 4.0 (*4*) for minor allele frequency (MAF) and

pathogenicity scores.

1264 Based on the prevalence of CHH (*5*), we established the MAF threshold as 0.01% and

excluded all variants with a higher MAF in gnomAD. Candidate *NOS1* variants were then

1266 prioritized using the following criteria: (i) *in silico* prediction of deleteriousness (CADD(*6,*

7) > 15), and (ii) variant position in sub-regions highly intolerant to variation (LIMBR(*8*)

1268 score percentile < 5). All variants were confirmed by Sanger sequencing of both strands

with duplicate PCR reactions. A gene burden analysis for the identified *NOS1* variants was

49

1270 performed using a two-tailed Fisher's exact test in CHH probands vs. controls (gnomAD exome controls). Furthermore, mutations in known CHH genes *(5, 9, 10)* according to

1272 ACMG criteria were noted for each proband and family members harboring rare variants in *NOS1*. More specifically, we evaluated coding exons and intronic splice regions (≤6 bp

1274 from the exons) of the known CHH genes for pathogenic and likely pathogenic variants according to ACMG guidelines (*11*). The included CHH genes were: *ANOS1*

1276 (NM_000216.2)*, SEMA3A* (NM_006080)*, FGF8* (NM_033163.3)*, FGF17* (NM_003867.2)*, SOX10* (NM_006941)*, IL17RD* (NM_017563.3)*, AXL* (NM_021913)*, FGFR1*

1278 (NM_023110.2)*, HS6ST1* (NM_004807.2)*, PCSK1* (NM_000439)*, LEP (*NM_000230), *LEPR* (NM_002303)*, FEZF1 (*NM_001024613)*, NSMF* (NM_001130969.1)*, PROKR2*

1280 (NM_144773.2)*, WDR11* (NM_018117)*, PROK2* (NM_001126128.13)*, GNRH1* (NM_000825.3)*, GNRHR* (NM_000406.2)*, KISS1* (NM_002256.3)*, KISS1R*

1282 (NM_032551.4)*, TAC3* (NM_013251.3)*, and TACR3* (NM_001059.2).

Position-specific evolutionary preservation tool (PANTHER-PSEP) (*12*) was used to

1284 determine whether the identified *NOS1* missense variants were at sites conserved among species, including pig, rabbit, rat, mouse and ferret (GenBank accession numbers

1286 F1RKF2, O19132, D3ZEW7, Q9Z0J4 and M3XUN6 respectively) and to predict their putative damaging effect.

1288

In silico analysis

1290 The ConSurf web server (http://consurf.tau.ac.il) was used for the identification of evolutionary conservation of amino acid positions in human NOS1 (*13*). The degree of

1292 amino acid evolutionary conservation reflects its natural tendency to be mutated. The aim of the method was to investigate whether any of the identified mutations are important for

1294 structure and/or function based on the evolutionary pattern of Nos1. A homology sequence search was conducted based on amino acid sequence from the human crystal structure

1296 of NOS1 (PDB ID code: 5VUV). PSI-BLAST homolog search algorithm and UniProt database were used for the generation of a Multiple Sequence Alignment (MSA) with

50

1298 ClustalW algorithm and homologs were selected automatically. Maximum of 50

sequences, closest to the reference sequence of Nos1, was used for the analysis out of

1300 the homolog search algorithm. Maximal and minimal % ID between sequences were set

at 95 and 35 respectively.

1302

Production of NOS1 constructs

1304 A cDNA containing the entire coding region of the human *NOS1* transcript isoform 1

(RefSeq. NM_000620.4; GenBank assembly accession; GRCh37.p13 /

1306 GCF_000001405.25), was inserted into a modified pcDNA3.1+ expression vector

containing a his-tag at the 5'end (GeneCust). Similarly, plasmid encoding *NOS1* mutants

1308 (Arg260Gln and Ile1223Met) were obtained using modified pcDNA3.1+ expression vector

containing a myc-tag at the 5'end of the coding region (GeneCust). The plasmids encoding

1310 remaining *NOS1* mutants (p.Ala231Thr, p.Thr1107Met and p.Glu1124Lys) were

generated by site-directed mutagenesis using QuickChange XLII Kit (Stratagene) and

1312 confirmed by Sanger sequencing. FlincG3 NO-detector plasmid (pTriEx4-H6-FGAm) has

been produced as described previously (*14*).

1314 To express equimolar amounts of WT and mutated *NOS1* transcripts in transfected cells,

we engineered bicistronic expression vectors encoding His-tag NOS1 and Myc-tag NOS1

1316 separated by a P2A self-cleaving peptide to achieve equimolar expression of WT and

mutated NOS1 at single cell level (*15*). Briefly, the His-NOS1 WT cassette was PCR-

1318 amplified and fused via overlap PCR to a synthetic P2A DNA sequence. The resulting His-

NOS1wt-P2A cassette was cloned (EcoRI – NotI) into pcDNA3.1+ expression vector.

1320 Next, sequences encoding for Myc-tag NOS1 mutants were PCR amplified adding NotI

and XbaI restriction sited. PCR products were finally cloned (NotI – XbaI) to His-NOS1wt-

1322 P2A expression vectors. PCR amplifications were performed using Phusion HF (Thermo

Fisher Scientific) or Herculase (Agilent Technologies) high-fidelity DNA polymerases using

1324 primers listed in Table S3. All vector sequences were validated by Sanger sequencing.

Compounds used for in vitro and in vivo experiments

All of the compounds used were delivered to the HEK 293T cells through superfusion. To explore the ability of the transfected cell line respond to nitric oxide, cells were treated with the NO donor (Z)-1-[N-(3-ammoniopropyl)-N-(n-propyl)amino] diazen-1-ium-1,2-diolate (PAPA/NO; 1µM, Enzo Life Sciences) for 90 sec. Endogenous NO release was stimulated through application of calcimycin (A23187; 50 nM diluted in DMSO, Abcam) for 1 min. The responses to NO could be inhibited by both the NOS inhibitor (L-NAME; 30 µM, Calbiochem) and the NO receptor blocker 1H-[1,2,4]oxadiazolo[4,3,-a] quinoxalin -1-one (ODQ; 1 µM, Sigma-Aldrich). ODQ is shown to selectively and potently inhibit guanylyl cyclase and thus it can block the accumulation of cGMP in response to NO donors (*16*). For in vivo application, NO synthesis was blocked using the NOS blocker L-NAME (Merck, Ref. 483125; 50 mg/kg i.p. and 5 mM intranasally), diluted as previously described (*17*). The activity of phosphodiesterase 5 (PDE5) was inhibited by the use of sildenafil (Sigma-Aldrich, Ref. PZ0003; 15 mg/kg, i.p.) diluted in DMSO. KINOX 450 ppm mole/mole inhaled nitric oxide gas was generously supplied by the Lille University Hospital.

Cell culture of NO detector cells

The HEK 293T cell line expressing NO-activated GC and PDE5, previously referred to as GChighPDE5low cells (*18*) and hereby referred to as NO detector cells, were provided by D. Koesling (Ruhr-Universitat Bochum). HEK 293T were cultured under standard conditions in a DMEM-based medium containing 5% fetal bovine serum and appropriate selection antibiotics; they were replated before reaching 80% confluency and were passaged<35 times.

Transfection was performed on cells growing in a 12-well plate (on poly-D-lysine-coated coverslips) for live cell imaging, or in a 6-well plate for NOS activity assay kit (Abcam; Cat. # ab211084) and co-immunoprecipitation experiments, using Fugene6 (Roche Applied Science) according to the manufacturer's protocol, at a transfection rate of 3:1

(Fugene6/DNA). For the live-cell imaging, Flincg3 plasmid was co-transfected, in a one

1354   step process, with the *NOS1* plasmid used in each experiment.

1356   **Western blot protein expression assay**

HEK293 cells were transfected in 12-well plates (2.5×10^5 cells/well) with WT, mutant

1358   NOS1 and bicistronic constructs (500ng/well) using Fugene6 (Roche Applied Science)

according to the manufacturer's protocol, at a transfection rate of 3:1 (Fugene6/DNA).

1360   After 48h, proteins were extracted and Western blot performed loading 20ug per lane.

NOS1 and actin were revealed using anti-myc tag HRP conjugated (1:5000; Bethyl Cat#

1362   A190-105P, RRID:AB_162712) or the anti-his tag (1:5000; Cell Signaling Technology

Cat# 2365, RRID:AB_2115720), and the anti-Actin (1/5000; Cell Signaling Technology

1364   Cat# 4970, RRID:AB_2223172) respectively.

1366   **Live imaging**

FlincG3 fluorescence imaging: FlincG3 has a broad excitation spectrum with peaks at

1368   491 and 410 nM and an emission maximum at 507 nm. Time series were recorded using

an Axio Observer Z1, with a camera (Orca LT) and a 20X air objective (numerical aperture

1370   0.8, Zeiss), under software control (Zen Imaging Software, Zeiss). Fluorescent HEK 293T

cells were excited at a wavelength set at 495, with an emission set at 519. Exposure levels

1372   were set at 300 ms and the intensity level at 8%. The chamber was superfused at 1.5

ml/min and temperature set at 37°C with imaging solution containing: KCl 2 mM, KH2PO4

1374   1.18 mM, glucose 5.5 mM, HEPES 10 mM, NaCl 140 mM, CaCl2 1.5 mM. The solution

was adjusted to a pH of 7.4 and osmolality to 285-290 mOsmol/kg at a temperature of

1376   37°C.

FlincG3 fluorescence data analyses: Epifluorescent signals were captured by camera,

1378   corrected for the background levels, and displayed as the change in intensity relative to

baseline divided by the baseline intensity ($\Delta F/F_o$). Peak amplitudes for each cell giving a

1380   fluorescent signal were measured by taking the maximum $\Delta F/F_o$, subtracting the mean

baseline and then subtracting the difference between the peak $\Delta F/F_o$ of the baseline and

1382   the mean baseline for that cell, as previously described (*14, 18*). These calculations were

made with OriginPro software (RRID:SCR_014212).

1384

NOS activity assay

1386   The enzymatic activity of the NOS1 protein was assessed in NO detector cells transfected

with the wild-type or the mutated plasmids, or transfected with the bicistronic constructs

1388   using a commercially available Abcam NOS activity assay kit (Cat. # ab211084) according

to the manufacturer's instructions.

1390

Protein immunoprecipitation assay

1392   NO detector cells expressing the wild-type NOS1 or each of the bicistronic constructs stated above

were lysed in Tris buffer pH 8.0 (25mM Tris base, 300mM NaCl, 50mM imidazole) with the addition

1394   of the protease and phosphatase inhibitor cocktail (Sigma-Aldrich, Cat. # PPC1010). Histidine-

tagged NOS1 was isolated using the Dynabeads His-tag isolation and pulldown kit (Invitrogen, Cat.

1396   # 10103D). Briefly 2mg of Dynabeads were added into 35µg of cell lysate and the Dynabeads-

lysate mix was then incubated in a roller at 4 $^{\circ}$C for 10min. The beads were thoroughly washed four

1398   times in the Tris buffer using a magnet and eventually any protein bound to the his-tag was eluted

using Tris buffer pH 8.0 containing increased concentration of imidazole (25mM Tris base, 300mM

1400   NaCl, 500mM Imidazole). Protein content was measured in the whole lysate (i.e. prior to elution),

as well as in the eluted part, using a BCA kit, according to the manufacturer's instructions. For the

1402   immunoblot of the whole lysate and the eluted proteins, loading buffer (E-Gel™, 1X, Thermo Fisher

Scientific, Cat. # 10482055) was added to the 5mg of each protein sample. The mix was then boiled

1404   for 5 min before electrophoresis at 120V for 100 mins in 5–12% tris-acetate precast SDS-

polyacrylamide gels according to the protocol supplied with the NuPAGE system (Thermo Fisher

1406   Scientific). After size fractionation, the proteins were transferred onto a polyvinylidene difluoride

membrane (0.2µm pore size, LC2002; Invitrogen) in the blot module of the NuPAGE system

1408   maintained at 1A for 75 min at room temperature (RT). Blots were blocked for 1h in tris-buffered

saline with 0.05% Tween 20 (TBST) and 5% non-fat milk at RT, incubated for 48h at 4°C with anti-

54

his-tag mouse monoclonal (1:1000; Thermo Fisher Scientific, Cat # MA1-21315, RRID:AB_557403), rabbit anti-NOS1 (1:1000; Thermo Fisher Scientific Ca t# 61-7000, RRID:AB_2313734) and rabbit anti-GAPDH (1:5000; Sigma-Aldrich Cat # G9545, RRID:AB_796208) in TBST 5% bovine serum albumin (Sigma-Aldrich, Cat # A7906), and washed four times with TBST before being exposed to horseradish peroxidase-conjugated secondary antibodies [anti-mouse Ig-HRP 1:1000 (Agilent Cat# P0260, RRID:AB_2636929) and anti-rabbit Ig-HRP 1:2000 (Agilent Cat# P0448, RRID:AB_2617138)] diluted in 5% non-fat milk TBST for 1h at RT. The immunoreactions were detected with enhanced chemiluminescence (NEL101; Perkin Elmer).

Animals

All C57Bl/6J mice were housed under specific pathogen-free conditions in a temperature-controlled room (21-22°C) with a 12h light/dark cycle and ad libitum access to food and water. Experiments were performed on male and female C57BL/6J mice (Charles River Laboratories), *Nos1*-deficient (*Nos1*$^{-/-}$, B6.129S4-Nos1tm1Plh/J, RRID:IMSR_JAX:002986) mice[19] and *Gnrh*::*Gfp* mice (a generous gift of D.J. Spergel, Section of Endocrinology, Department of Medicine, University of Chicago) [20]. *Nos1*$^{-/-}$; *Gnrh*::*Gfp* mice were generated in the animal facility of the PLBS UAR 2014 – US41 (https://ums-plbs.univ-lille.fr/) by crossing *Nos1*$^{-/+}$ mice with *Gnrh*::*Gfp* mice. Animal studies were approved by the Institutional Ethics Committees for the Care and Use of Experimental Animals of the Universities of Lille, Bordeaux and Geneva; all experiments were performed in accordance with the guidelines for animal use specified by the European Union Council Directive of September 22, 2010 (2010/63/EU) and the Swiss Federal Act on Animal Protection Ordinance, and were approved by the French Department of Research (APAFIS#2617-2015110517317420v5 and #27300-2020092210299373v3) and the Swiss Animal Protection.

Gonadectomy in mice

The gonadectomy of wild-type C57Bl/6J mice was performed either at P12 or at 13 weeks of age under general isoflurane anesthesia (induction 4% in air 2 L/min, then 1.5% in air 0.3 L/min) after local injection of lidocaine (30 microliters of a 0.5% solution, subcutaneously.) and preemptive meloxicam treatment (5 mg/kg). Infantile mice were euthanized at P23 and adults two weeks thereafter.

Examination of physiology

Weaned female mice were checked daily for vaginal opening. After vaginal opening, vaginal smears were collected daily and analyzed under the microscope to identify the onset of puberty (first appearance of two consecutive days where vaginal smears contained cornified cells) and eventually the specific day of the estrous cycle. Male mice were checked daily for balanopreputial separation, as an external sign of puberty onset.

In utero intranasal injection of L-NAME

Pregnant wild-type female mice were anesthetized with isoflurane, placed ventral side up and covered with a sterile surgical cloth. Abdominal hair was removed from a small surface around the incision. Skin and connective tissue were carefully cut and a small incision in the abdominal wall allowed the exposure of the uterine horn. Each horn was carefully pulled out of the abdomen and placed on top of it, while it was kept moist with fresh DPBS throughout the surgical process. Saline and the NOS inhibitor L-NAME (5mM) were injected into contralateral horns of each pregnant female. The needle was positioned vertically over the nose of the E12.5 embryo, and introduced until it was estimated to reach the nasal septum. Following administration of the substance, the needle was held steady for a few seconds before being gently withdrawn. The uterus was then returned to the abdomen and rehydrated with a small amount of DPBS. The incisions were closed with surgical sutures and the female was singly housed until embryo harvesting (E14.5).

Intraperitoneal injection of L-NAME in infantile mice

56

1466   P10 wild-type female mice received twice-daily injections of L-NAME (50 mg/kg, i.p.) or
control saline, during the infantile period, until the day of weaning (P21). L-NAME or the

1468   saline control were administered at 8H00 and 18H00, one hour after lights on and one
hour before lights off according to a previously described protocol (*17*). At the end of the

1470   treatment with the NOS inhibitor, mice were monitored for the assessment of pubertal
onset and the study of estrous cyclicity (see "Examination of physiology" section above).

1472   When L-NAME treated mice and their control littermates reached adulthood, blood
samples were collected from the facial vein on diestrus I and proestrus for the

1474   measurement of LH hormone concentrations (described below).

1476   **Hormone concentration measurements**

Plasma LH was measured using a highly sensitive enzyme-linked Immunosorbent assay

1478   (ELISA) as described elsewhere (*21*). Serum FSH concentrations were measured using
radioimmunoassay as previously described (*22*). The accuracy of hormone

1480   measurements was confirmed by the assessment of rodent serum samples of known
concentration (external controls). Serum 17β-estradiol concentration was determined by

1482   ELISA (Demeditec Diagnostics, Cat# DE2693) as described previously (*23*). Inhibin B was
measured using a commercial ELISA multispecies kit (AnshLabs, Cat # AL-163), following

1484   the manufacturers' protocol. AMH was measured using the commercial rat and mouse
AMH ELISA kit (AnshLabs, Cat# AL-113) as described elsewhere (*24*).

1486

Inhaled NO administration

1488   The protocol was adapted from previous publications (*25, 26*). $Nos1^{+/-}$ mother and her
pups ($Nos1^{+/+}$, $Nos1^{+/-}$ and $Nos1^{-/-}$) were placed inside a cage ("inhaled NO chamber")

1490   constantly perfused with 20 ppm NO, a dose commonly administered to premature infants
at birth (*27*) that induces the production of cGMP (fig. S7). Treatment started when pups

1492   reached P10 (lights on) and ended at P23, when mice were weaned and removed from
the inhaled NO chamber.

1494

Sildenafil administration

1496 P10 *Nos1*$^{+/+}$, *Nos1*$^{+/-}$ and *Nos1*$^{-/-}$ mice received daily injections of the phosphodiesterase 5 inhibitor sildenafil (15 mg/kg, i.p.) during the infantile period, until the day of weaning (P23).

1498 Sildenafil was administered at 8H00, one hour after lights were turned on. At the end of the treatment with the NOS inhibitor, mice were monitored for the assessment of vaginal

1500 opening, pubertal onset and balanopreputial separation (see "Examination of physiology" section above).

1502

Cognition, olfaction, and hearing behavioral tests

1504 For all behavioral tests, the animals were coded so that the investigator was blinded to the genotype/phenotype of each animal.

1506 ***Novel object recognition test:*** Recognition memory was assessed using the novel object recognition (NOR) test. During the habituation phase on day 1, each mouse was allowed

1508 to explore the open-field arena for 30 minutes. On day 2, two identical objects (A+A) were placed within the open-field arena on opposite sides of the cage, equidistant from the cage

1510 walls. Each mouse was placed within the two objects and allowed to explore them for 15 minutes. Day 3 consisted of two phases, a familiarization and a test phase. During the

1512 familiarization phase (trial 1) that lasted 15 minutes, mice explored two other identical objects (B+B). After this phase, the mouse was placed back in its home cage for 1 hour

1514 before starting the test phase. During the test phase, one object of trial 1 and a completely new object (B+C) were placed within the open-field area and mice were allowed to explore

1516 them for 5 minutes (trial 2). The object recognition score was calculated as the time spent exploring the new object (trial 2) over the total exploration time, and is used to represent

1518 recognition memory function. NOD was performed in the afternoon in 3- to 8-month-old male and female mice; females were in diestrus during the test phase.

1520 ***Olfactory habituation-dishabituation test****:* The habituation-dishabituation test was used to assess the ability to differentiate between different odors. This olfactory test included a

58

1522   presentation of acetophenone (Sigma-Aldrich, Cat. # 00790) for habituation and octanol

(Sigma-Aldrich, Cat. # 05608) for dishabituation, or vice versa. Before the test, mice were

1524   allowed to explore the open-field area and an empty odor box for 30 minutes. After this

habituation period, mice were sequentially presented with one odor for four consecutive

1526   trials for a duration of 1 minute, and an inter-trial interval of 10 minutes was maintained to

ensure the replacement of the odor. After four consecutive trials, a second odor was

1528   presented during a 1-minute trial. Odors (20µl of 1:1000 dilution) were administered on a

filter paper and placed in a perforated plastic box, to avoid direct contact with the odor

1530   stimulus. Measures consisted in recording the total amount of time the mouse spent

sniffing the object during the different trials. Habituation-dishabituation testing was

1532   performed in the morning in 3- to 8-month-old male and diestrous female mice.

Social olfactory preference test*:* The social olfactory preference test consisted of two

1534   phases, a familiarization and a test phase. During the familiarization phase, all mice were

allowed to freely explore the open-field arena and were exposed to urine samples from an

1536   adult C57BL6/J wild-type stud male and estrous female for 30 min. After 30 min in clean

bedding, mice were allowed to explore the same urine samples for 10 min, during which

1538   the behavior towards the urine samples was recorded. For each test, 50 µl of either male

or female urine was administered on a filter paper and placed in a perforated plastic box,

1540   to avoid direct contact with the odor stimulus. The distribution of the time sniffing the urine

samples was used as an indication of the interest to gain further information from the scent

1542   source. Social olfactory preference test was performed in the morning in 3- to 8-month-old

male and female mice; females were in estrous during the test phase.

1544   ***Hearing tests:*** Mice were anesthetized by intraperitoneal injection of a mixture of a

ketamine and levomepromazine (100 mg/kg and 5 mg/kg respectively) and placed on a

1546   servo-controlled heating pad that maintained their core temperature at 37°C. Audiological

tests were performed in a sound-proof booth. Distortion-product otoacoustic emissions

1548   (DPOAES) probes cochlear mechanics and auditory brainstem-evoked response (ABR)

thresholds and suprathreshold waveforms, both of which are used to detect auditory-

1550 pathway disorders. The predominant DPOAE at frequency $2f_1$-f_2 was recorded in response

to two primary tones f_1 and f_2, with f_2/f_1 = 1.20, at equal sound levels (Cub^{e}Dis system,

1552 Mimosa Acoustics; ER10B microphone, Etymotic Res.). Frequency f_2 was swept at 1/10th

octave steps from 4 to 20 kHz, and DPOAE level was plotted against frequency f_2 at

1554 increasing primary tone levels, from 20 to 70 dB SPL in 10 dB steps, then to 75 dB SPL.

The ABRs elicited by calibrated tone bursts in the 5-40 kHz range (repetition rate 17/s)

1556 were derived by synchronously averaging electroencephalograms recorded between

subcutaneous stainless-steel electrodes at the vertex and ipsilateral mastoid, with the help

1558 of a standard digital averaging system (CED1401+). One hundred 10-ms long epochs

were averaged, except within 10 dB of the ABR threshold (defined as the smallest tone-

1560 burst level giving rise to at least one repeatable wave above background noise level, 100

nV in an anesthetized mouse), for which 300 epochs were collected. Next, ABRs in

1562 response to 10-kHz tone bursts at increasing levels, stepwise from 15 to 105 dB were

collected and their waves were labelled from I to IV in chronological order, for the latency

1564 of wave II to be extracted at every stimulus level. Hearing tests were performed during the

whole day in 2- to 3-month-old male and diestrus female mice.

1566

Attentional set shifting task

1568 The attentional set shifting (ASST) apparatus and procedures were previously described

in detail (*28*). In brief, testing was performed in a homemade rectangular chamber made

1570 of Plexiglas and white PVC, 40 x 30 x 40 cm. A 15 x 30 cm area of the chamber was

separated in the middle by an opaque white PVC separation, on each side of which a

1572 texture and a digging bowl (made of ceramic 3 cm height x 8 cm diameter size) were

placed. In all ASST trials, two odorants presented as clean odorized bedding in two bowls

1574 and two textures presented below each bowl were randomly combined and

counterbalanced, and placed in two separate compartments of the testing chamber.

1576 Various spices and herbs bought in a grocery store were used as odorants and were

added to the digging medium (the volume of each odorant was mostly 0.5 % of the volume

1578   of the digging medium prepared at least 24 hours before use). Various textures were used

as a second sensory dimension. Each texture material was cut to obtain rectangles of

1580   similar sizes (about 18 x 14 cm) and uniform thickness. These textures were matched by

color to avoid visual bias during testing.

1582   In each trial, only one cue, either an odor or a texture, is reinforced by a food reward

hidden in the bedding (TestDiet; 20 mg sucrose pellet – Chocolate 1811223). For each

1584   trial, mice were allowed a maximum of five minutes to give an answer. The mouse was

requested to meet the learning criterion, which is 80% correct choice rate over 10

1586   consecutive trials, and at least the six last trials had to be consecutively correct choices,

to pass each block within a maximum of 90 trials. The relevant dimensions were

1588   counterbalanced.

The mouse was placed on a restricted diet from at least three weeks before the ASST.

1590   Around one gram of food was provided per mouse per day to maintain the mouse above

85% of the initial free-feeding body weight. Before starting the ASST habituation, at least

1592   five days were used to stabilize their weight. The degree of hunger could be a potential

confounding factor that may affect the duration and number of trials. The body weight was

1594   thus measured every morning and evening. The quantity of daily restricted food was

strictly controlled until the day the mouse terminated all blocks of the ASST.

1596   At least 5 days before the ASST, the mouse started habituating to the empty testing

chamber for 30 minutes on three consecutive days. On the fourth day, the mouse started

1598   to habituate to dig two bowls filled with bedding, and a reward (TestDiet; 20 mg sucrose

pellets) was added on each side of the separating wall to train the mouse to dig for a

1600   reward.

The ASST was conducted on two consecutive days. On day one, the mouse performed

1602   the simple discrimination (SD), the compound discrimination (CD) and the reversal of CD

(CDR) blocks. On day two, the mouse performed the intradimensional set-shifting (IDS)

1604   and the extradimensional set-shifting (EDS) blocks.

The odorant bedding-filled digging bowls were placed on each side of the separating wall.

1606 The bowls were placed on texture. The bowl on the side containing the relevant and correct dimension (either odorant or texture) contained a 20 mg food pellet. After the mouse was

1608 placed on the waiting chamber, the trial with the recording started. The trial ended, and its result recorded until the mouse finished having the reward sucrose pellet. If a correct

1610 choice was made, the mouse was allowed to consume the reward and then returned to the waiting chamber of the testing chamber; in case of an incorrect choice, the mouse was

1612 directly returned to the waiting chamber. If no choice was made after five minutes, the trial was considered incorrect, and the mouse had to return to the waiting chamber. For the

1614 first three trials, the mouse was permitted to dig in the unbiased bowl without consequence, although an error was recorded, so that if one bowl was investigated in

1616 error, the mouse could move to the second baited bowl and learn the cue contingency. The location (left/right) of the digging bowls and combinations of two different textures and

1618 two different odors were pseudo-randomly changed between trials so that the mouse would not associate an odor to a texture or the correct choice to the location of the

1620 chamber. During testing, the chamber was cleaned using 70 % ethanol, and textures were cleaned after every trial. When the mouse reached a learning criterion, the next block, a

1622 new set of cues was presented, and a positive transfer of the learned rule was expected; [the mouse had to make a new reward cue association within the same relevant sensory

1624 dimension as in the previous block (the SD, CD, CDR or IDS block)]. After reaching the learning criterion again, the next block, another set of cues was used, and a new reward-

1626 cue association was made by reinforcing a cue within the previously irrelevant dimension (the EDS block), that is, testing the negative transfer of a previously learned rule. A

1628 perseverative response is the continuation of a choice made based on a previously learned rule. Where the total number of trials needed by a mouse to meet a given criterion

1630 is X, and the number of errors that the mouse makes during the first half of the trials (X/2), that is, when a learned choice can be expected to persist, is Y, the perseverative error can

1632 be calculated as 2Y/X.

62

iDISCO+ and tissue transparentization

1634   *Sample preparation*: P0 pups coming from *Nos1*$^{+/-}$ mothers were anesthetized and perfused with a fixative solution made up of 4% paraformaldehyde in PBS. The heads

1636   were postfixed in the fixative overnight, then rinsed with PBS, and subsequently decalcified in an acidic solution (10% formic acid in ddH2O) before removal of the frontal

1638   and parietal bones.

Whole-mount immunostaining and tissue-clearing: An adapted iDISCO+ protocol was

1640   performed: samples underwent a gradual dehydration in ethanol, followed by overnight delipidation in 66% dichloromethane (DCM) / 33% ethanol, two rinses in ethanol, and

1642   overnight bleaching in 7% H2O2 in ethanol. Samples were then rehydrated gradually in ethanol and washed in potassium phosphate-buffered saline (KPBS). Next, the heads

1644   were blocked and permeabilized in blocking solution (KPBS + 0.2% gelatin + 1% Triton X-100 + 0.05% sodium azide) for 5 days, and incubated with primary antibodies rat anti-

1646   GnRH (1:10000 #EH1044, produced by E. Hrabovszky) and goat anti-TAG1 (1:500, R and D Systems Cat# AF4439, RRID:AB_2044647) in blocking solution for 10 days. After

1648   several KPBS rinses, the heads were incubated with secondary antibodies in blocking solution for 5 days, and rinsed again several times in KPBS. After immunostaining, the

1650   samples were gradually dehydrated in ethanol and left overnight in dichloromethane 66% / ethanol 33%. The samples were finally rinsed in 100% dichloromethane for 1 hour,

1652   before clearing in dibenzyl ether until transparency was achieved.

Light-sheet imaging and 3D-analysis: Cleared samples were imaged in dibenzyl ether

1654   on an Ultramicroscope 1 (LavisionBiotec) equipped with an Andor Neo camera and a 1.1x/0.1NA MI PLAN objective (LavisionBiotec). Acquisitions were saved as a tiff

1656   sequence, which was converted to the Imaris file format and further processed in Imaris 9.6 (Bitplane RRID:SCR_007370). The Spots tool was used for GnRH neurons counting.

1658

Immunohistochemistry and immunofluorescence

1660   *Mouse*

Tissue preparation: Embryos were washed thoroughly in cold 0.1 m PBS, fixed in fixative solution [4% paraformaldehyde (PFA), in 0.1 m PBS, pH 7.4] for 6–8 h at 4°C and cryoprotected in 20% sucrose overnight at 4°C. The next day, embryos were embedded in OCT cryoembedding matrix (Tissue-Tek), frozen on dry ice, and stored at −80°C until sectioning. Tissues were cryosectioned (Leica cryostat) sagitally at 16 µm.

Postnatal (P7 to P23) wild-type female mice were anesthetized with 50-100 mg/kg of Ketamine-HCl and perfused transcardially with 2-10 ml of saline, followed by 10-50 ml of 4% PFA, pH 7.4. Brains were collected, postfixed in the same fixative for 2h at 4°C, embedded in OCT embedding medium (Tissue-Tek), frozen on dry ice, and stored at −80°C until cryosectioning (Leica cryostat). Sections were collected coronally at 35µm (free-floating sections) and 16µm for iNO box post-weaning *Nos1*$^{+/-}$ mice.

Wild-type adult intact and gonadectomized mice were injected i.p. with a mixture of pentobarbital (300 mg/kg) and lidocaine (30 mg/kg) and perfused transcardially with 2-10 ml saline followed by 200 ml of 2% PFA in PB, pH 7.4, containing 0.2% picric acid. Brains were collected, cryoprotected overnight in a sucrose solution (20% in a 0.1M veronal buffer (VB), pH 7.4), embedded in Tissue-Tek, frozen in liquid nitrogen and stored at -80°C until cutting onto a cryostat (Microm). Twelve-micrometer thick coronal sections were collected onto gelatinized slides and kept at -80°C until immunolabeling.

Immunolabeling of NOS1 and P-NOS1/ cGMP neurons in mouse developing hypothalamus: As described previously (*17, 29*), sections were washed 3 times for 15 minutes each in PB 0.1M and then incubated in blocking solution (5% NDS, 0.3% Triton X-100 in PB 0.1M) for 1 hour at room temperature. Sections were incubated for 72 hours at 4°C with rabbit anti-Ser1412 phospho-Nos1 (1:500; Thermo Fisher Scientific Cat# PA1-032, RRID:AB_325020) and sheep anti-NOS1 (1:3000; generous gift from P.C. Emson, The Babraham Institute, RRID:AB_2895154) or sheep antiserum to formaldehyde-fixed cGMP (1:1000; H.W.M. Steinbusch, Maastricht University). Sections were rinsed in PB and then incubated 1h at room temperature with biotinylated donkey anti-rabbit (1:500; Jackson ImmunoResearch Laboratories Cat# 711-065-152, RRID:AB_2340593) followed

64

1690   by incubation for 1h at room temperature with streptavidin-Alexa 568 (1:500; Thermo Fisher Scientific Cat# S-11226) and Alexa 647 donkey anti-sheep (1:500; Thermo Fisher Scientific Cat# A-21448, RRID:AB_2535865), diluted in PB 0.1M. Sections were then

1692   rinsed and counterstained with Hoechst (0.0001% in PB 0.1M; 5 min), rinsed again and coverslipped under Mowiol.

1694   ***Immunolabeling of NOS1 and NK3R neurons in mouse hypothalamus***: As described previously (*17, 29*), sections were washed in 0.1M veronal buffer, pH 7.4 (VB) and

1696   incubated overnight at room temperature in a cocktail of sheep anti-NOS1 (1:5000; generous gift from P.C. Emson, The Babraham Institute, RRID:AB_2895154) and rabbit

1698   anti-NK3R [1:5000; (P. Ciofi, INSERM, RRID:AB_2868390), which allows the selective visualization in the arcuate nucleus of kisspeptin neurons by labeling their somatodendritic

1700   domain (*30*)) in VB containing 0.25% Triton X-100 (VB-TX) and 1% normal donkey serum. After washes in VB, sections were incubated for two hours at room temperature in a

1702   cocktail of Alexa 488 donkey anti-sheep (1:1000) and TRITC donkey anti-rabbit (1:1000) (both from Jackson ImmunoResearch Laboratories) in VB-TX. Sections were then rinsed

1704   and coverslipped under a 1:3 mixture of VB and glycerol, containing 0.1% para-phenylenediamine (Sigma-Aldrich).

1706

    Adult human brains

1708   ***Tissue preparation***: Human hypothalamic tissues from four male (aged 35, 36, 61 and 83 ys) and six female (aged 33, 58, 60, 70, 88 and 90 ys) patients were obtained at

1710   autopsies (post mortem interval<24 h) from the Forensic Medicine Department of the University of Debrecen, with the permission of the Regional Committee of Science and

1712   Research Ethics (DEOEC RKEB/IKEB: 3183-2010). The included patients were not known to suffer from neurological or endocrine disorders before death. Dissection and

1714   immersion-fixation of hypothalamic tissue blocks, section preparation of serial coronal sections covering also the infundibular region were carried out as previously described

1716   (*31*).

Peroxidase immunolabeling of NOS1 and P-NOS1 neurons in adult human

1718 ***hypothalamus:*** Dissection and immersion-fixation of hypothalamic tissue blocks, section

preparation and immunohistochemical procedures were adapted from a previous

1720 study (*32*). NOS1-synthesizing neurons were detected with a sheep NOS1 antiserum

(1:15,000, gift from P.C. Emson, The Babraham Institute, RRID:AB_2895154) and P-

1722 NOS1 neurons with a rabbit anti-Ser1412 phospho-Nos1 antiserum (1:100; Thermo Fisher

Scientific Cat# PA1-032, RRID:AB_325020). A 48h incubation in these primary antibodies

1724 was followed by working dilutions of biotinylated secondary antibodies (1:500; 1 h;

Jackson ImmunoResearch Laboratories) and then, ABC Elite reagent (1:1000; 1 h ; Vector

1726 Laboratories). The signal was visualized with nickel-diaminobenzidine (Ni-DAB). To study

the relationship between NOS1 and GnRH neurons, the Ni-DAB signal was silver-gold-

1728 intensified (*32*), followed by the detection of GnRH neurons with a guinea pig GnRH

antiserum (1:50,000; 48h ; #1018 produced by E. Hrabovszky), biotin-SP–anti-guinea pig

1730 IgG (1:500; 1h ; Jackson ImmunoResearch Laboratories), ABC Elite reagent (1:1000; 1 h;

Vector Laboratories) and DAB chromogen.

1732 ***Triple-immunofluorescent detection of kisspeptin, NOS1 and GnRH in adult human***

brains: Biotin Immunofluorescence experiments were performed as reported previously

1734 (*31*). For simultaneous triple-immunofluorescent labelling of NOS1, GnRH and kisspeptin,

previously characterized primary antibodies were applied to the sections in a cocktail

1736 consisting of rabbit kisspeptin (1:1000; Antibody Verify Inc., Las Vegas, NV; Cat#

AAS26420C, targeting amino acids 21–81) (*33*), sheep NOS1 (1:1000, gift from P.C.

1738 Emson, The Babraham Institute, RRID:AB_2895154) and guinea pig GnRH (1:1000;

#1018 produced by E. Hrabovszky) (*32*) antisera (4C; 24h). Then, the sections were

1740 transferred into a cocktail of antirabbit- Cy3 (1:1000) +anti-sheep-FITC (1:250) + anti-

guinea pig-Cy5 (1:500) secondary antibodies (Jackson ImmunoResearch Laboratories)

1742 for 12 h at 4 °C. The triple-labeled specimens were mounted, coverslipped with Mowiol

and analyzed with confocal microscopy (Zeiss LSM780 microscope). High resolution

1744 images were captured using a 20×/0.8 NA objective, a 1–3× optical zoom and the Zen

software (Carl Zeiss). Different fluorochromes were used and detected with the following

1746   laser lines: 488 nm for FITC, 561 nm for Cy3, 633 nm for Cy5.

Emission filters were as follows: 493–556 nm for FITC, 570–624 nm for Cy3 and 638–759

1748   nm for Cy5. To avoid the emission crosstalk between the fluorophores, the red channel

(Cy3) was recorded separately from the green (FITC)/far-red (Cy5) channels ('smart setup'

1750   function). To illustrate the results, confocal Z-stacks (Z-steps: 0.941-1.000 μm, pixel dwell

time: 1.27-1.58 μs, resolution: 1024×1024 pixels, pinhole size: set at 1 Airy unit) were

1752   used. The extent of colocalization between kisspeptin and NOS1 was estimated from four

postmenopausal patients (aged 58, 70, 88 and 90 ys), known to exhibit the highest

1754   kisspeptin levels in the infundibular region (*32*).

1756   **Digital image acquisition of mouse sections**

Immunofluorescent preparations were analyzed on the LSM 710 Zeiss confocal

1758   microscope. Excitation wavelengths of 493/562 nm, 568/643 and 640/740 were selected

to image Alexa 488, Alexa 568 and Alexa 647 secondary antibodies. All images were

1760   taken with the objective EC Plan-Neofluar M27 (thread type). To investigate GnRH

neuronal migration in embryonic tissue, sagittal sections of the head were acquired with

1762   the 20X objective, using a numerical aperture 0.50, and a zoom of 1.0. To analyze the

hypothalamic NOS1/p-NOS1 ratio during development, Z-stack images were acquired

1764   with the 40X oil objective, using a numerical aperture of 0.50, and a zoom of 1.0. For the

analysis of hippocampal NOS1/p-NOS1 ratio after ovariectomy, Z-stack images with tiles

1766   were acquired with the 20X objective, using a numerical aperture of 0.80, and a zoom of

1.0 All images were captured in a stepwise fashion over a defined z-focus range

1768   corresponding to all visible staining within the section and consistent with the

optimum step size for the corresponding objective and the wavelength. Two-

1770   dimensional images presented here are maximal intensity projections of three-

dimensional volumes along the optical axis. Illustrations were prepared using Adobe

1772 Photoshop (Adobe Systems).

1774 **Cell counting**

Analysis was undertaken by counting the numbers of single-labeled, dual-labeled (NOS1

1776 staining colocalizing with p-NOS1). The number of the above Nos1- expressing neuronal

populations were counted in the region of organum vasculosum lamina terminalis (OVLT),

1778 represented by plate 16, of the L.W. Swanson brain map (*34*) as described previously (*35*).

All the above values for each mouse were used to determine mean counts for each age

1780 group which were then used to generate mean + SEM values for each group. Embryonic

tissue sagittal sections of the brain were examined in a Zeiss Axio Imager Z2 microscope.

1782 Alexa 488 was imaged by using a 495 beam splitter with an excitation wavelength set at

450/490 and an emission wavelength set a 500/550, allowing the identification of

1784 immunocytochemically labeled GnRH neurons. All GnRH neuronal nuclei throughout each

tissue section were visualized and counted.

1786

Isolation of hypothalamic GnRH neurons using fluorescent-activated cell sorting

1788 To obtain single-cell suspensions the preoptic region of *Nos1*$^{-/-}$; *Gnrh*::*Gfp*; mice was

microdissected and enzymatically dissociated using a Papain Dissociation System

1790 (Worthington Biochemical Corporation). FACS was performed using an EPICS ALTRA

Cell Sorter Cytometer device (BD Bioscience). The sort decision was based on

1792 measurements of GFP fluorescence (excitation: 488nm, 50 mW; detection: GFP

bandpass 530/30 nm, autofluorescence bandpass 695/40nm) by comparing cell

1794 suspensions from *Gnrh*::*Gfp* and wild-type animals. For each animal, about 200 GFP-

positive cells were sorted directly into 10µl extraction buffer: 0.1% Triton® X-100 (Sigma-

1796 Aldrich) and 0.4 U/µl RNaseOUT™ (Life Technologies).

1798 **Quantitative RT-PCR analyses**

68

mRNAs obtained from FACS-sorted GnRH neurons or pituitary tissues were reverse

1800 transcribed using SuperScript® III Reverse Transcriptase (Life Technologies) and a linear

preamplification step was performed using the TaqMan® PreAmp Master Mix Kit protocol

1802 (P/N 4366128, Applied Biosystems). Real-time PCR was carried out on Applied

Biosystems 7900HT Fast Real-Time PCR System using exon-boundary-specific

1804 TaqMan® Gene Expression Assays (Applied Biosystems): *Gnrh1* (Gnrh1-

Mm01315605_m1), *Gnrhr* (Mm00439143_m1), *Cebpb* (Mm00843434_s1). Control

1806 housekeeping genes: *r18S* (18S-Hs99999901_s1), *ACTB* (Actb-Mm00607939_s1).

1808 **Brain slice preparation and electrophysiology**

Infantile *Nos1$^{+/+}$*;*Gnrh::Gfp* and *Nos1$^{-/-}$*; *Gnrh*::*Gfp* littermates (P13-P20) were

1810 anaesthetized with isoflurane, and, after decapitation, the brain was rapidly removed and

put in ice-cold oxygenated (O_2 95% / CO_2 5%) artificial cerebrospinal fluid (ACSF)

1812 containing the following (in mM): 120 NaCl, 3.2 KCl, 1 NaH_2PO_4, 26 $NaHCO_3$, 1 $MgCl_2$, 2

$CaCl_2$, 10 glucose, pH 7.4 (with O_2 95% / CO_2 5%). After removal of the cerebellum, the

1814 brain was glued and coronal slices (150 μm thickness) were cut throughout the septum

and preoptic area using a vibratome (VT1200S; Leica). Before recording, slices were

1816 incubated at 34ºC to recover for 1 h. After recovery, slices were placed in a submerged

recording chamber (32.8ºC; Warner Instruments) and continuously perfused (2 ml/min)

1818 with oxygenated ACSF. *GFP*-positive GnRH neurons in the hypothalamic preoptic area

were visually identified with a 40 X objective magnification in an upright Leica DM LFSA

1820 microscope under a FITC filter and their cell body observed by using IR-differential

interference contrast. Whole-cell patch-clamp recordings were performed in current-clamp

1822 with bridge mode by using a Multiclamp 700B amplifier (Molecular Devices). Data were

filtered at 1 kHz and sampled at 5 kHz with Digidata 1440A interface and pClamp 10

1824 software (Molecular Devices). Pipettes (from borosilicate capillaries; World Precision

Instruments) had resistance of 6-8 MΩ when filled with an internal solution containing the

1826 following (in mM): 140 K-gluconate, 10 KCl, 1 EGTA, 2 Mg-ATP and 10 HEPES, pH 7.3

with KOH. Bridge balance was adjusted to compensate for pipette resistance. All

1828　recordings were analyzed with Clampfit 10 (Molecular Devices). Junction potentials were

determined to allow correction of membrane potential values. Electrical membrane

1830　properties were measured in current-clamp mode by applying a series of current pulses

from – 60 to + 80 pA (1 s, 10 pA increments). Input resistance (R_{in}) was determined by

1832　measuring the slope of the linear portion of the current-voltage (I-V) curve. All data are

presented as mean ± standard deviation.

1834
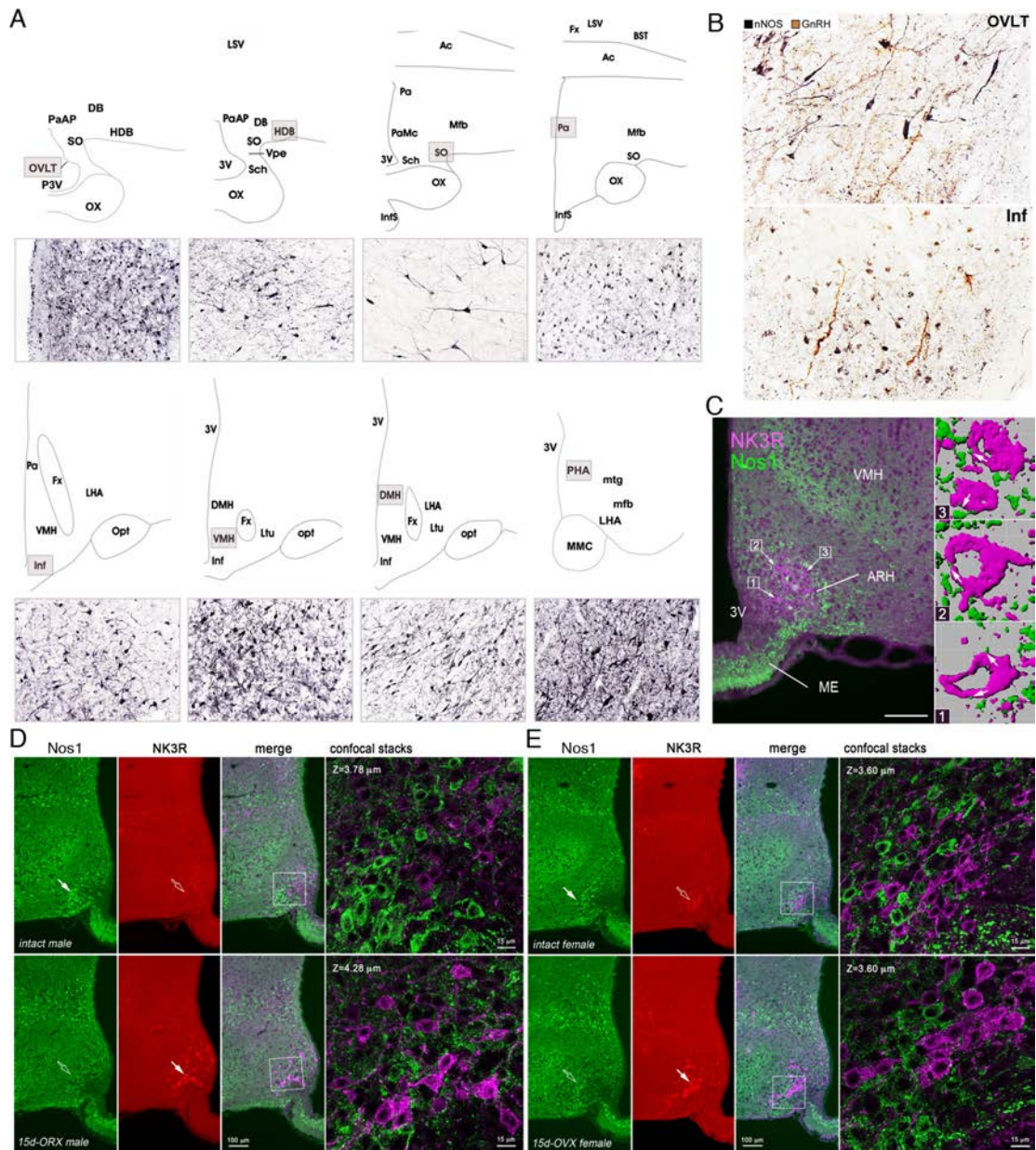
Figure S1. **NOS1 expression in the GnRH neuronal system in humans and mice.** (A) Distribution of NOS1-immunoreactive neurons (purple labeling) throughout the adult hypothalamus in human. (B) Anatomical relationship between NOS1 neurons (purple) and GnRH neurons (light brown) in the region of the organum vasculosum laminae terminalis (OVLT, upper panel) and the infundibulum (Inf, lower panel) in adult human hypothalamus. (C) Localization of Nos1 immunoreactivity with respect to the neurokinin B receptor (NK3R)-immunoreactive kisspeptin neurons in the arcuate nucleus (ARH) of the hypothalamus in mice. Separate neurons display labeling for Nos1 (green) and NK3R (magenta), but their interaction is visible under the form of putative Nos1-contacts onto

NK3R-somatodendritic domains (arrows in insets numbered 1-3). *Left*, video camera image of a 12 μm-thick section. *Right*, surface renderings of confocal optical sections, 1μm-thick over a 10μm-grid. (D,E) Nos1 and NK3R immunoreactivities in intact and 2-week gonadectomized adult males (D) and females (E). Ac, anterior commissure; BST, bed of the stria terminalis; DB, diagonal band of Broca; DMH, dorsomedial hypothalamic nucleus; fx, fornix; HDB, horizontal limb of the diagonal band; LHA, lateral hypothalamic area; LSV, lateral septal nucleus mfb, medial forebrain bundle; LTu, lateral tuberal nucleus; MMC, medial mammillary nucleus; mtg, mammillo-tegmental tract; opt, optic tract; ox, optic chiasma; Pa, paraventricular nucleus; PaAP, paraventricular nucleus anterior parvicellular; PaMC, paraventricular nucleus magnocellular part; PHA, posterior hypothalamic area; Sch, suprachiasmatic nucleus; SO, supraoptic nucleus; VMH, ventromedial hypothalamic nucleus; 3V, third ventricle. Bar, 100 μm in (A) and (C), and 50 μm in (B).
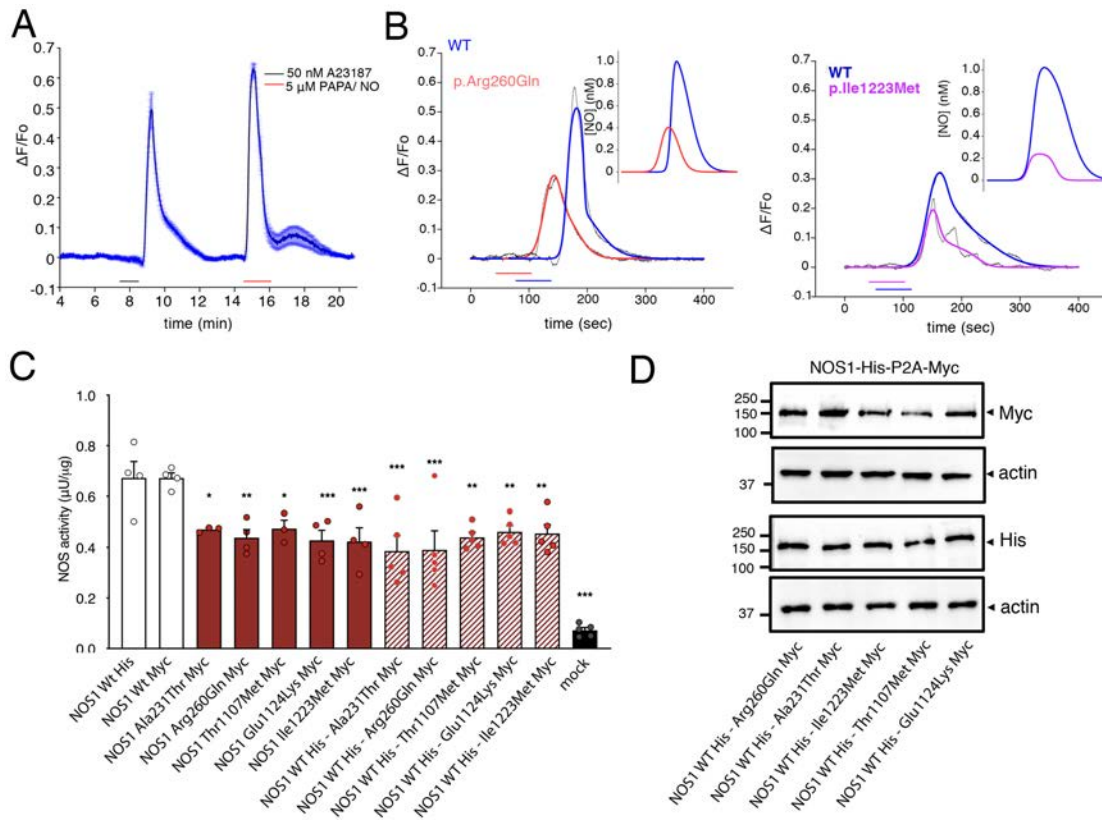
72

Figure S2. Functional assays of the NOS1 mutants in vitro. (A) Demonstration of the experimental protocol routinely used for testing the different NOS1 variants: Superfusion of the calcium ionophore A23187 (50 nM) elicited a seemingly rapid fluorescence response that reached a peak within the first minute of the application in cells expressing the wild-type plasmid efore recovering to baseline values on washout. Superfusion of a high concentration of the NO donor PAPA/NO (5 μM) allowed us to estimate the peak of the A23187-evoked increase in fluorescence using the published concentration-response curve parameters in FlincG3-transfected HEKGC/PDE5 cells. Data are means of different cells recorded from the same coverslip (n>20 for each experiment). (B) Representative illustrations of the behavior of FlincG3-transfected HEKGC/PDE5 cells co-transfected with the wild-type or mutated NOS1 in response to application of the A23187. Mutants are illustrated in comparison to wild-type cells from the same experiment (transfection and imaging). The color-coded line (wild-type NOS1 is represented in blue and mutants are each in a different color) fits the data to the GC/PDE5 model previously published. The inset illustrates the attempts to describe NO generation using the Mathcad model, which are in good agreement with those calculated using the Hill equation (data not shown). The similarities in the shapes of the derived NO concentration profiles indicate that the time-

courses for the mutants are similar to wild-type, suggesting reduced net NO synthesis as opposed to altered activation kinetics. Note that NO release was not observed in cells not containing any NOS1 construct, while it was abolished in the presence of the guanylate cyclase inhibitor ODQ (1 µM) (data not shown). (C) Measurement of the enzymatic activity (µU/µg) of the NOS1 protein detected in HEK GC/PDE5 cells expressing the wild-type (white bars), or the mutated (identified variants -red bars- or the bicistronic plasmids -dashed bars-) NOS1 protein, or in cells not transfected (that is, mock cells, black bars) using a commercially available kit. Mutants are compared to wild-type values (one-way ANOVA with Dunnett's post-hoc test, n=4,4,3,4,3,4,4,5,5,5,5,5,5). * $P < 0.05$; ** $P < 0.01$; *** $P < 0.001$. Values indicate means ± SEM. N >3 independent experiments using technical replicates; each dot represents an independent experiment including technical triplicates. (D) Representative Western blots showing Myc-tagged NOS1 mutants with His-tagged WT NOS1 in cells transfected with the bicistronic NOS1-His-PA-NOS1-Myc plasmid. Actin immunoblot was used as loading control.
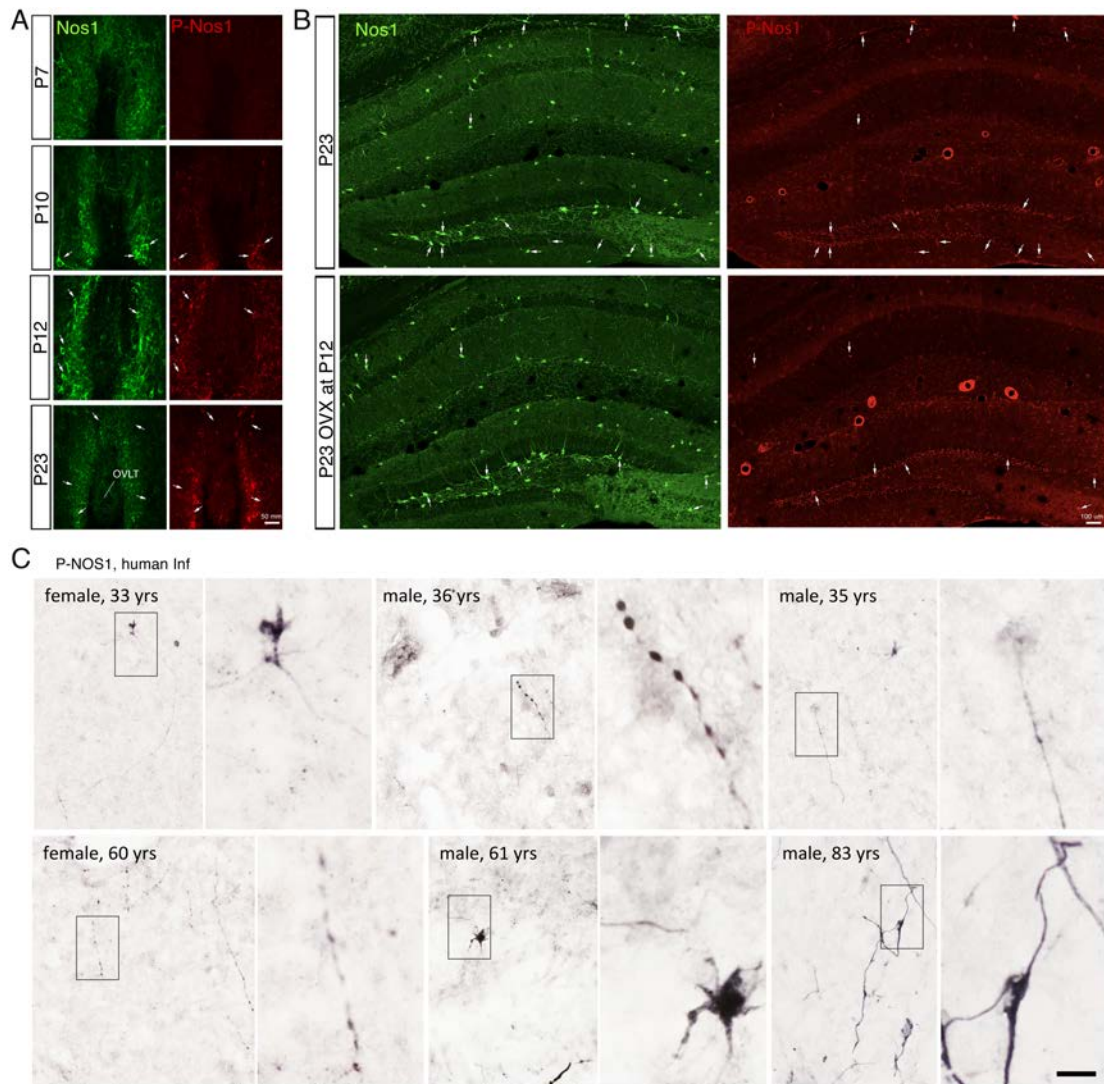
1898

Figure S3. Immunofluorescent images of the Nos1 / P-Nos1 labeling in various areas of the mouse and human brain. (A) Progressive phosphorylation of the Nos1 protein during postnatal development in the preoptic region at the level of the organum vasculosum of the lamina terminalis (OVLT) leads to activation of the NO pathway at postnatal day 12. Nos1 (green) and P-Nos1 (red) immunoreactivity in forebrain coronal sections of the OVLT in female mice during pre-pubertal postnatal day 7, 10, 12, and 23. (B) Ovariectomy at p12 blunted the increase in the phosphorylation of Nos1 at P23 in the hippocampus. (C) Representative images showing NOS1 Ser1412 phosphorylation immunolabeling in the adult hypothalamus of women and men at different ages.

1908
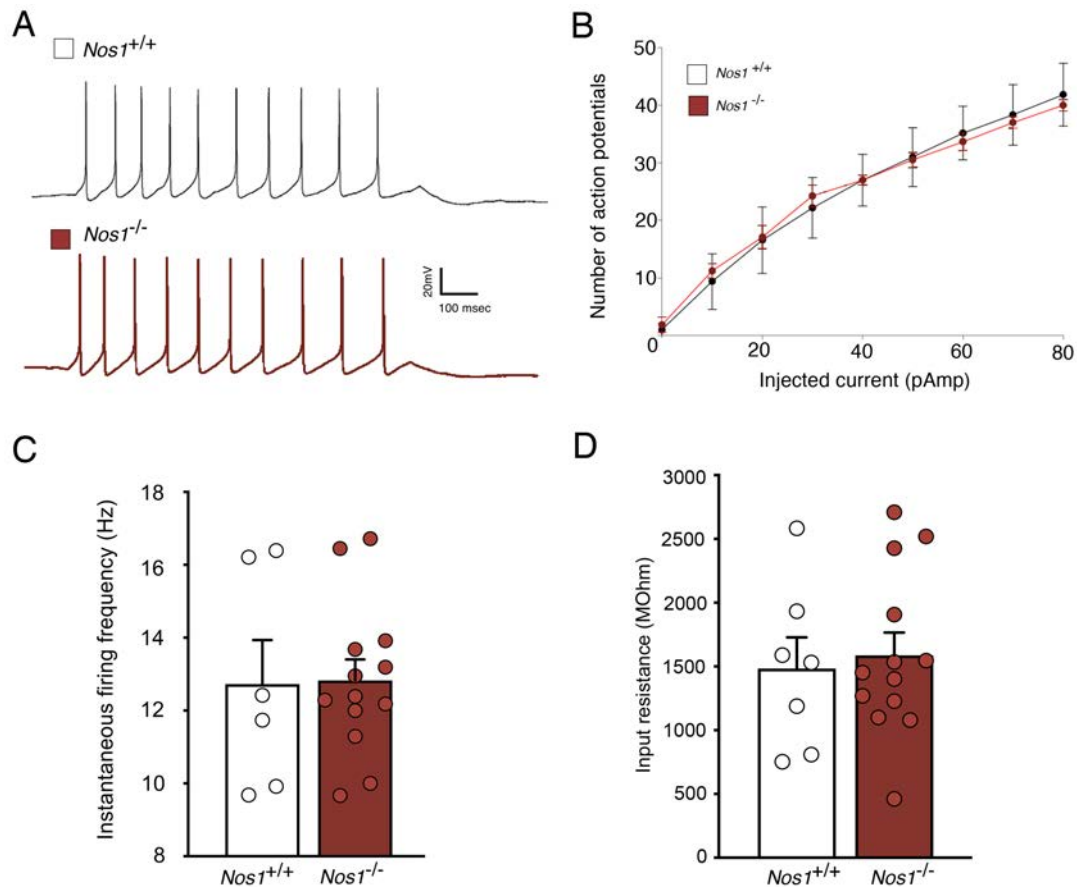
Figure S4. The evoked firing response of GnRH neurons does not differ between *Nos1*+/+ and *Nos1*-/- animals. (A) Representative traces of firing evoked by a 10pA current injection in GnRH neurons from *Nos1*+/+ (top trace) and *Nos1*-/- (bottom trace in brown) mice. (B) Frequency-Current curve of evoked firing response in GnRH neurons from *Nos1*+/+ (white) and *Nos1*-/- (brown) mice over a range of current injections. (C) Instantaneous firing frequency (1/1st interspike interval) after 10pA current injection in GnRH neurons (*n*=6,13) from *Nos1*+/+ (white) and *Nos1*-/- (brown) animals (N=5,6). (D) Input resistance in GnRH neurons (*n*=7,13) from *Nos1*+/+ (white) and *Nos1*-/- (brown) animals (N=5,6). Values indicate means ± SEM. Animals were from at least 3 independent litters.
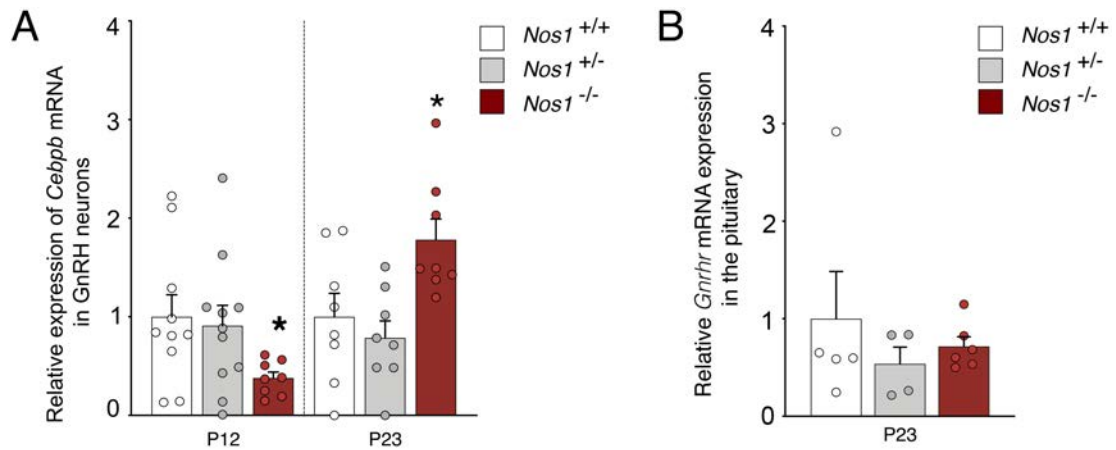
1922

Figure S5. NOS1-deficiency alters the infantile expression of the *Gnrh* promoter repressor *Cebpb* in GnRH neurons isolated by FACS, but not *GnrhR* expression in the pituitary. (A) *Cebpb* transcript expression in GnRH neurons at P12 and P23 in wild-type and NOS1-deficient mice. *Gnrh::Gfp; Nos1*^{+/+} (white) values are compared to those of *Gnrh::Gfp; Nos1*^{+/-} (grey) and *Gnrh::Gfp; Nos1*^{-/-} (brown) mice (one-way ANOVA with Dunnett's post-hoc test; P12: *n*=10,11,8; P23: *n*=8,8,8) * $P<0.05$. Values indicate means ± SEM. N=5-8 independent litters. (B) *Gnrhr*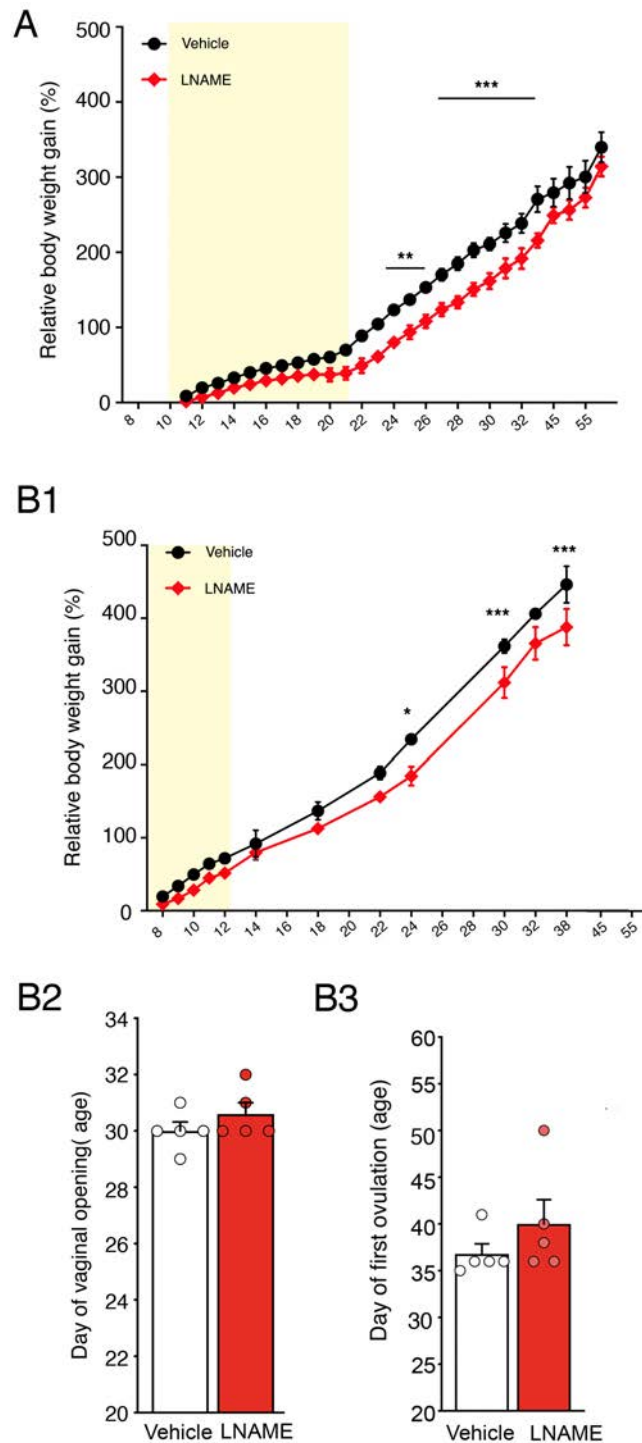 transcript expression in the pituitary at P23 in wild-type (white) and Nos1-deficient (*Nos1*^{+/-} in grey and *Nos1*^{-/-} in brown) mice (*n*=5,4,6). Values indicate means ± SEM. N>3 independent litters.

1932

1934

Figure S6. Pharmacological inhibition of NO synthesis during the beginning of the infantile period (P7- 12) leads to a decrease in body weight but has no effect on the sexual maturation. Examination of relative body weight gain (A,B1) of mice treated daily with vehicle or L-NAME (red) between P10 and P23 (A, n=10,9) or P7 and P12 (B1, n=5,6). In the latter group of mice vaginal opening (B2) and pubertal onset in female mice (B3) were also analyzed (n=5,5). Vehicle-treated animals are compared with L-NAME-injected littermates using multiple t-test with Holm-Sidak correction (A) or unpaired t-test (B2,B3).

78

* *P* < 0.05; ** *P* < 0.01; *** *P*<0.001. Values indicate means ± SEM. N>3 independent
1944   litters.

1946
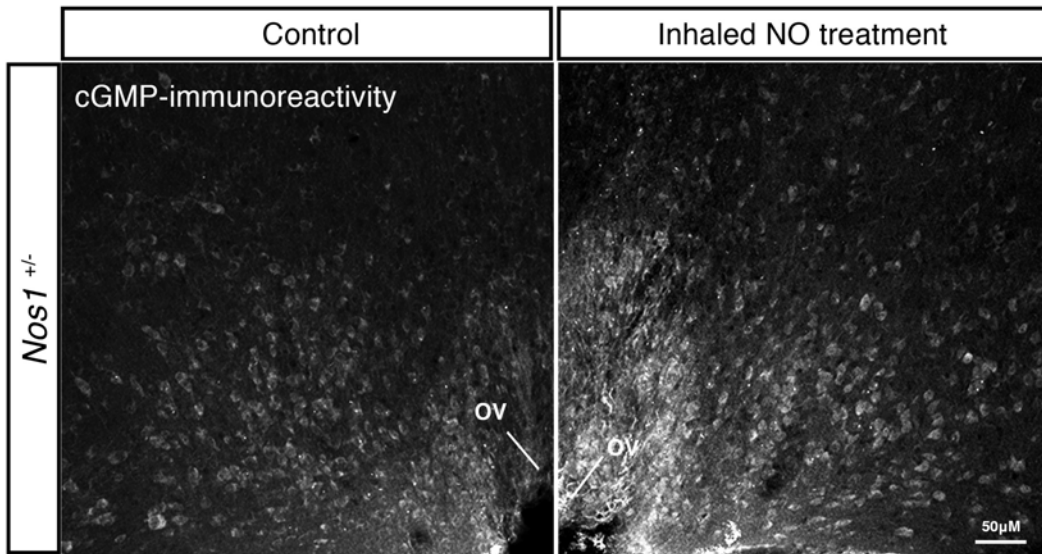
Figure S7. Representative immunofluorescent images showing increased cGMP content in the OVLT of P23 Nos1$^{+/-}$ male mouse after inhaled NO treatment. Immunostaining against cGMP (white) in coronal sections (16μm) from the OVLT region of a control (left panel) and inhaled NO treated (right panel) Nos1$^{+/-}$ male mouse. Pups treated with inhaled NO have been exposed with the whole litter to 20 ppm NO from P10 to P23. Scale bar: 50 μm.

1960 **Table S1: Genetic and functional characterization of *NOS1* rare sequence variants in CHH**

patients

NOS1 mutations	MAF in gnomAD exome datasets			Allelic count			Regional constraint	Protein prediction		
HGSV	gnomAD	gnomAD (controls)	gnomAD (controls) MaxPop	CHH M / W	gnomAD M / W	Fisher test (p value)	LIMBR (percentile)	CADD	PP2	SIFT2
c.691G>A [p.Ala231Thr]	absent	absent	absent	1 / 681	0 / 108486	0.0062	4.35%	15.01	B	T
c.779G>A [p.Arg260Gln]	0.003%	0.002%	0.006% (Latino)	1 / 681	2 / 108058	0.0187	4.35%	23.6	B	T
c.3320C>T [p.Thr1107Met]	0.007%	0.006%	0.012% (Eu non Finn)	1 / 681	7 / 108615	0.0488	1.28%	29.9	D	D
c.3370G>A [p.Glu1124Lys]	0.005%	0.006%	0.014% (Eu non Finn)	2 / 680	6 / 108250	0.0011	1.28%	22.3	B	T
c.3669A>G [p.Ile1223Met]	absent	absent	absent	1 / 681	0 / 108627	0.0062	1.28%	24	P	T

1962 Nucleotide and protein changes are based on reference cDNA sequence NM_000620.4. CHH cohort included 341 patients. MAF, minor allele frequency. M/W, number of mutated/ wild type alleles.

Table S2: Statistical analyses by figure panel

1964

Table S3: Primers used for the production of His-NOS1-P2A-myc-NOS1 expression vectors

1966

Primer name	Sequence (5' – 3')
His-NOS1-F	GTCCAGTGTGGTGGAATTCGCC
His-NOS1-P2A-R	TCTCCTGCTTGCTTTAACAGAGAGAAGTTCGTGGCGGAGCTGAAAACCTCATCGG
myc-NOS1-F1	CGCTTCACGCGGCCGCTATGGAGCAGAAACTCATCTCTGAAG
myc-NOS1-F2	CGCTTCACGCGGCCGCTATGGAGCAAAAACTTATTTCAGAGG
myc-NOS1-R1	GACACCGATGAGGTTTTCAGCTCCTCTAGACGATTCAGG

1968 **Movie S1: iDISCO NOS1-immunoreactivity in a wild-type mouse**

Movie S2: iDISCO NOS1-immunoreactivity in a *Nos1* knockout mouse

1970 **Data file S1: Raw data for all figures where *n*<20 (provided as a separate Excel file)**

1972